



School of Chemistry

Plasma-assisted growth of continuous grain diamond by static flow CVD

Max Radbourne

**This thesis is submitted in partial fulfilment of the requirements for the Honours
Degree of Chemistry BSc at the University of Bristol**

Supervisor: Prof. Neil Fox
Second Assessor: Prof. PW May
Third Assessor: Prof. David Fermin

Statement of Factors which limited project progress

During the course of this project there were delays to the build due to lead times on certain vacuum fittings and molybdenum substrate materials having extended delivery times, leaving less time for planned experiments to be completed.

Abstract

The initial aim of this project was the synthesis and characterisation of microcrystalline diamond diodes, formed on non-diamond substrates to ascertain a method for making high quality diodes with reproducible electrical characteristics. These diodes have the capacity to revolutionise beta-voltaic devices, through incorporating the radioisotope into the diode structure rather than it being external. The wider objective is the large-scale production of these highly effective devices powered by tritium after their function has been demonstrated using carbon-14. This technology has vast potential in low-output long life devices such as in pacemakers or small satellites.

The mini-PDR is a static flow pulsed DC CVD reactor designed with this target in mind and is set to be deployed at the UK Atomic Energy Authority (UKAEA). Before the mini-PDR could be commissioned it was important that appropriate growth conditions were established, and a standard operating procedure was created. To achieve this the assembly of the mini-PDR reactor was completed and several test runs were carried out where the plasma stability was assessed through camera observation and monitoring of optical emission spectra. Due to an air leak into the reaction chamber of the mini-PDR no diamond was synthesised during this study, this is because it allowed nitrogen to enter and quench methane intended for diamond growth. This leak could not be resolved despite many attempts, this therefore prevented the comparison of films grown using this reactor which was a target of this project.

Despite this, a standard operating procedure for the reactor was produced and appropriate growth conditions were established; a power of 600 W was selected as this permitted the temperature of the substrate to be in the desired region for growth without causing the powered cathode to overheat. An operating power of 180 Torr was also used for the successful deposition of graphitic carbon confirmed via Raman Spectroscopy, it was concluded this carbon was graphitic due to the excess of nitrogen during growth. The functionality of the carbon -14 vial cracking assembly was also successfully tested, a key component of the mini-PDR.

Acknowledgements

I would like to thank my supervisor Neil Fox for his interest and support throughout this project as well as everyone in Bristol University diamond group for making me feel welcome and making my time as part of the group enjoyable. I would particularly like to thank Dr James Smith for all his time and effort in the lab throughout the course of this project and always being willing to help.

Contents

1. Introduction	6
1.1 Diamond- Structure and Properties.....	6
1.2 Diamond Synthesis	7
1.2.1 High Pressure- High temperature.....	7
1.2.2 Chemical Vapour Deposition.....	8
1.3 CVD Growth.....	9
1.3.1 CVD Gas Phase Chemistry	10
1.3.2 Hot filament CVD (HFCVD).....	12
1.3.3 Microwave Plasma Assisted CVD (MW PACVD)	13
1.3.4 Pulse & DC Plasma Assisted CVD (DC PACVD).....	14
1.4 Applications of Synthetic Diamond.....	15
1.4.1 Isotopically Pure Diamond	16
1.4.2 Boron Doped Diamond (BDD).....	17
1.5 Static Flow	18
2. Experimental	20
2.1 Project Aims.....	20
2.2 Mini-PDR.....	20
2.3 Characterisation	21
2.3.1 Optical Emission Spectroscopy	22
3. Results & Discussion	23
3.1 Hydrogen only Tests	23
3.2 Methane Containing Tests	25
4. Conclusions	32
4.1. Future Work	33
5. Appendices	34
5.1 Standard Operating Procedure	34
5.2 OES Data	42
6. Bibliography	43

1. Introduction

1.1 Diamond- Structure and Properties

Diamond has long been pre-eminent due to its scarcity and natural beauty. Aside from being an illustrious gemstone, diamond has many practical applications due to its impressive physical properties. Diamond is a crystalline allotrope of carbon with 4-coordinate carbon atoms arranged tetrahedrally within a cubic crystal structure (**Figure 1**). Carbon atoms are relatively small so form short range, very strong sp^3 hybridised covalent bonds giving rise to its distinct properties. In contrast graphite, another allotrope of carbon has a layered structure with weak crosslinks due to sp^2 bonding which allows for use as a lubricant. Under atmospheric conditions graphite is the more thermodynamically stable allotrope of carbon, only a large kinetic barrier prevents conversion from diamond to graphite.^{1,2}

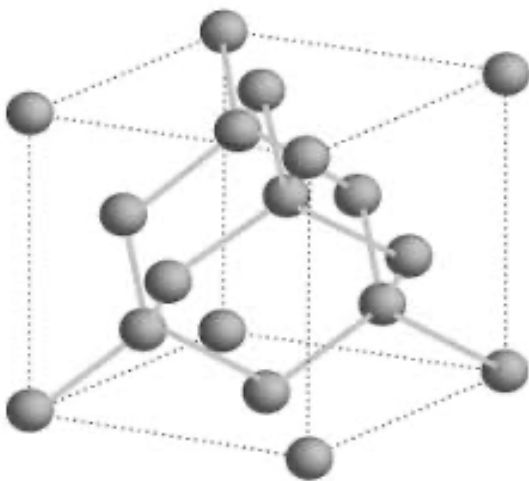


Figure 1. Diamonds cubic unit cell structure, demonstrating the short range sp^3 bonding which gives rise to its impressive physical properties.²

Table 1. Comparison of the physical properties of diamond with those of other group 14 elements.^{1,3-5}

	Diamond	Si	Ge
Density / g cm⁻³	3.5	2.3	5.3
Bulk Modulus / GPa	1200	100	75
Electrical Resistivity / Ω m	1×10^{14}	2.3×10^3	1
Thermal Conductivity / $W m^{-1} K^{-1}$	2×10^3	149	60.2
Bandgap / eV	5.47	1.12	0.67

The impressive physical properties of diamond when compared to other group 14 elements are demonstrated in **Table 1**.³⁻⁵ Diamonds high atomic density results in extreme mechanical hardness, exceptionally high thermal conductivity and unrivalled strength exemplified by the bulk modulus.¹ These distinctive properties make diamond sought after for applications such as in cutting tools and thermal management devices for example heat sinks.⁶ Diamond is a wide bandgap semiconductor with an incredibly high resistivity at room temperature, this combination makes an ideal candidate for use in various electrical components.¹ However, it is difficult to harness natural diamonds for use in this manner.

The use of lab grown diamond provides an alternative to this, chemically it is identical and therefore indistinguishable from natural diamond. Synthetic diamond not only offers a more ethical and economical means of obtaining gemstone diamonds but a means of harnessing diamond for use in active and passive electronics, particularly through doping with boron or nitrogen. This project will focus on the potential of synthetic diamond technology, in particular for the development of nuclear batteries which offers a solution to the recycling of hazardous nuclear waste through incorporation in the production of safe, long-life devices such as pacemakers.

1.2 Diamond Synthesis

1.2.1 High Pressure- High temperature

Diamond is naturally produced over 150 km below the Earth's surface as this region has the necessary temperatures and pressures to facilitate growth.⁷ The first synthetic diamonds were produced with this in mind, aiming to replicate these high-pressure, high-temperature conditions (HPHT) to convert graphite into diamond. HPHT synthesis was made industrially practical by the General Electric company in 1954.⁸ However, these early diamonds were coloured due to impurities and were therefore only suitable for industrial applications such as cutting tools rather than jewellery.

Modern HPHT synthesis utilises temperature gradient growth developed later in the 1950s. This involves exposing a graphite or diamond powder to pressures of 5-6 GPa and temperatures ranging from 1600 -1900 K in the presence of a metal catalyst (e.g. Fe-Ni) to allow lower temperature growth. As shown in the carbon phase diagram (**Figure 2**), under these conditions, diamond is stable and can spontaneously nucleate and grow due to graphite dissolving in the growth medium, forming a highly saturated carbon solution.^{9,10}

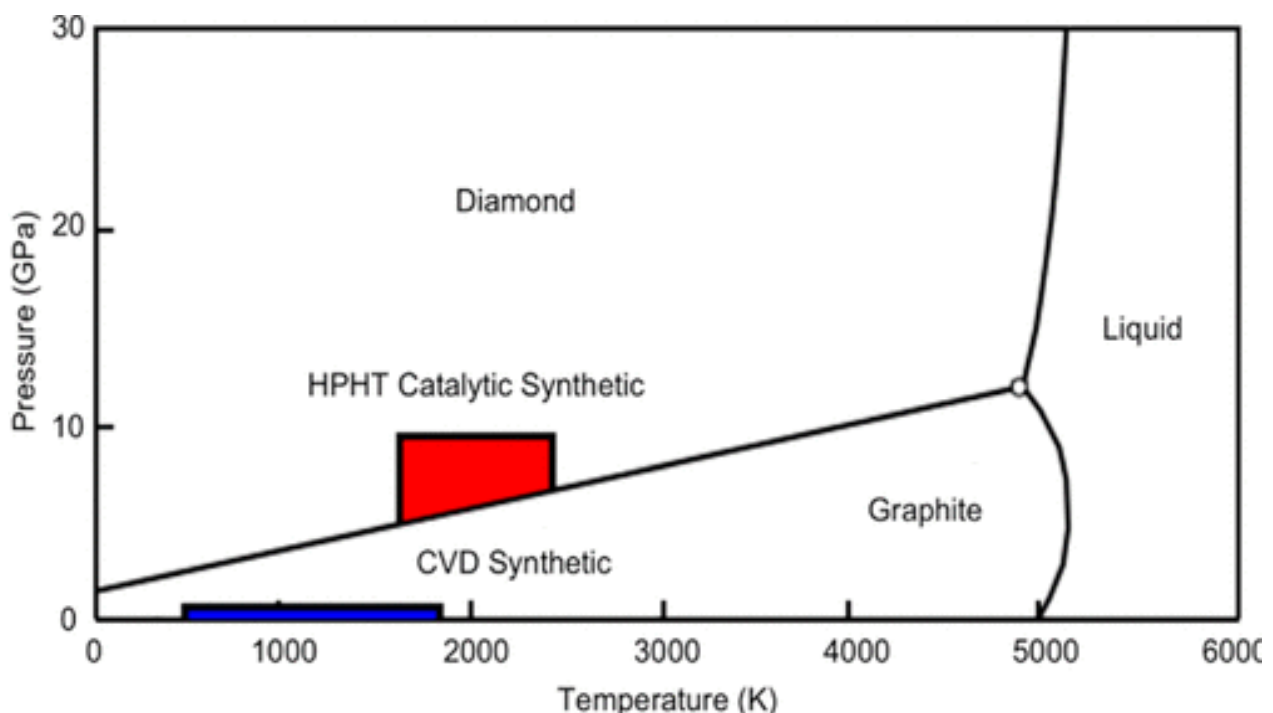


Figure 2. Carbon Phase diagram for carbon demonstrating the pressure and temperature at which HPHT and CVD synthesis can occur. (The area representing CVD growth has been inflated for clarity.)¹⁰

Development of HPHT growth methods have now allowed contamination levels to be controlled sufficiently to produce several colourless gems simultaneously. HPHT methods can now also be used to anneal pre-existing natural or synthetic diamonds to reduce the visible colouration and therefore increase their value. The main drawback of HPHT techniques is that it forms single crystals which cannot be selectively controlled in terms of dopants. Therefore, limiting the range of electrical applications for diamond produced in this manner.¹¹

1.2.2 Chemical Vapour Deposition

An alternative to HPHT synthesis, Chemical Vapour Deposition (CVD) has been widely studied since Matsumoto et al made breakthroughs in the early 1980s.¹¹ Driven by kinetics, nucleation is achieved under metastable conditions, a feat previously seen as implausible by theoretical arguments.¹² CVD growth is based on interactions between a carbon containing precursor gas above a suitable substrate leading to deposition.¹ CVD synthesis allows the impressive engineering potential of diamond to be utilised as films are produced with consistent characteristics and properties can be fine-tuned based on the desired application.¹³

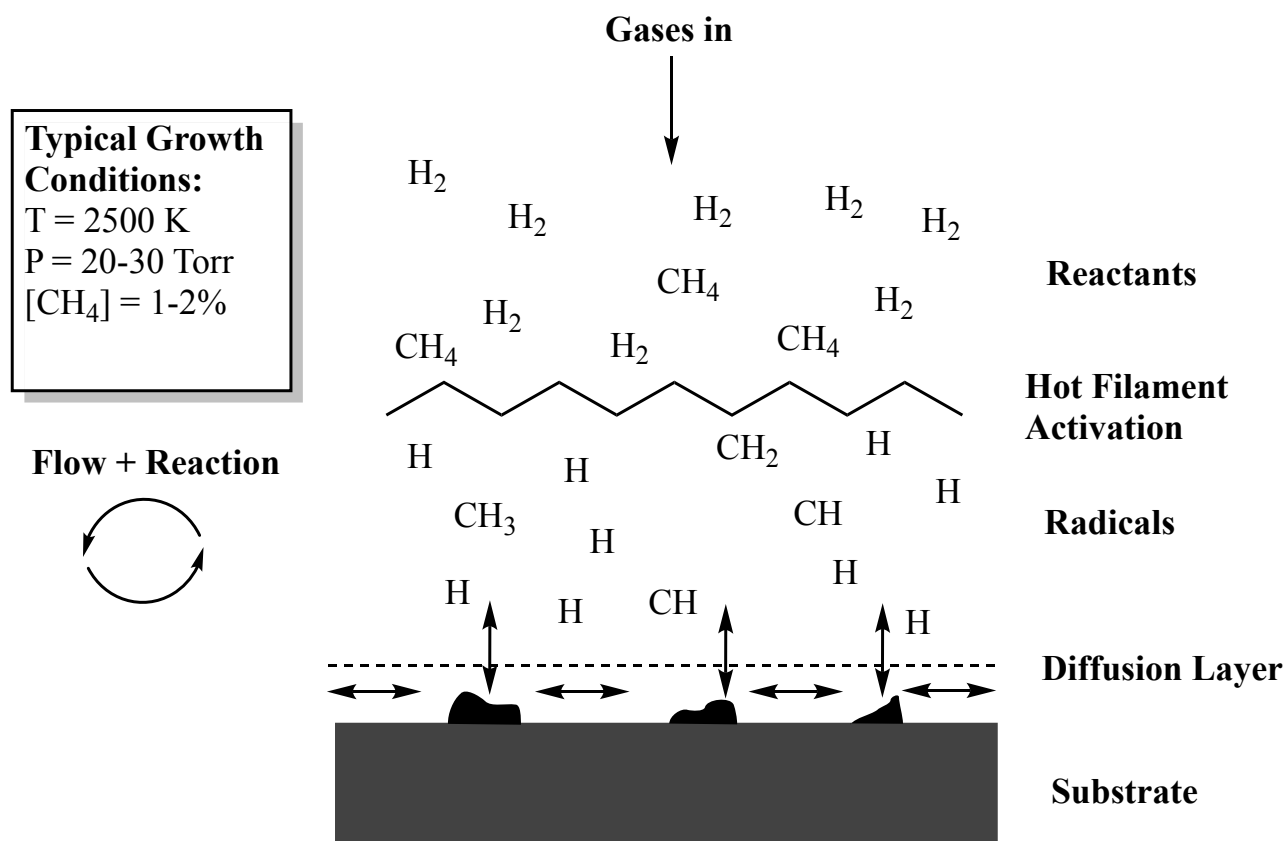


Figure 3. Schematic of the physical and chemical processes occurring during HFCVD with an inset of typical conditions used for this type of growth. Adapted from May¹¹

The most commonly used precursor gas for diamond film growth is methane and hydrogen, typically at a ratio of 1-2% CH₄. To initiate the growth process, the precursor gas must be activated, predominantly through thermal (**Figure 3**), combustion, or plasma methods, to form H atoms and methyl radicals. These fragments then undergo a series of reactions that lead to the diffusion and adsorption of the precursor molecules onto a suitable site on the substrate surface.¹⁴ The rate of deposition is highest when using combustion initiation, but crystals produced are lower quality due to lack of control and forming over very small areas. In contrast, thermal and plasma processes have much slower growth rates, but result in a much higher quality of film.¹⁵

1.3 CVD Growth

The growth process begins with the deposition of graphite, which contains small amounts of diamond. This deposited material is then selectively etched by atomic hydrogen, as diamond is more stable towards atomic hydrogen than graphite. In a diamond lattice, if two neighbouring carbon atoms are replaced by hydrogen, the sp^3 hybridisation remains unchanged. However, in graphite, the alteration of these bonds disrupts the entire ring. Therefore, the growth rate of diamond exceeds the etch rate, while the opposite occurs for graphite. Atomic hydrogen also prevents carbon cross-linking, thereby inhibiting the formation of graphite. It is therefore essential to enhance the formation of atomic hydrogen close to the substrate surface through optimising conditions such as temperature and pressure. The growth conditions play a crucial role in determining the properties of the resulting diamond film, including its thickness, texture, grain size, and the ratio of non-diamond carbon to diamond which can be quantitatively characterised by determining the sp^2 to sp^3 ratio.^{1,15,16}

The substrate used in CVD growth has a significant impact on the morphology of the resulting diamond. The use of single crystal diamond substrates results in homoepitaxial films, while using non-diamond substrates leads to heteroepitaxial growth. In the latter case, diamond growth originates from various nucleation sites, nuclei grow and gradually fuse with their neighbours to form a two-dimensional film which continues to propagate along the surface normal. The resulting film is typically polycrystalline, but process conditions dictate the morphology and average crystallite size. This can range from microcrystalline to ultranano-crystalline diamond, smaller grain sizes can be attained by increasing the C/H ratio of the precursor gas mixture.^{10,17}

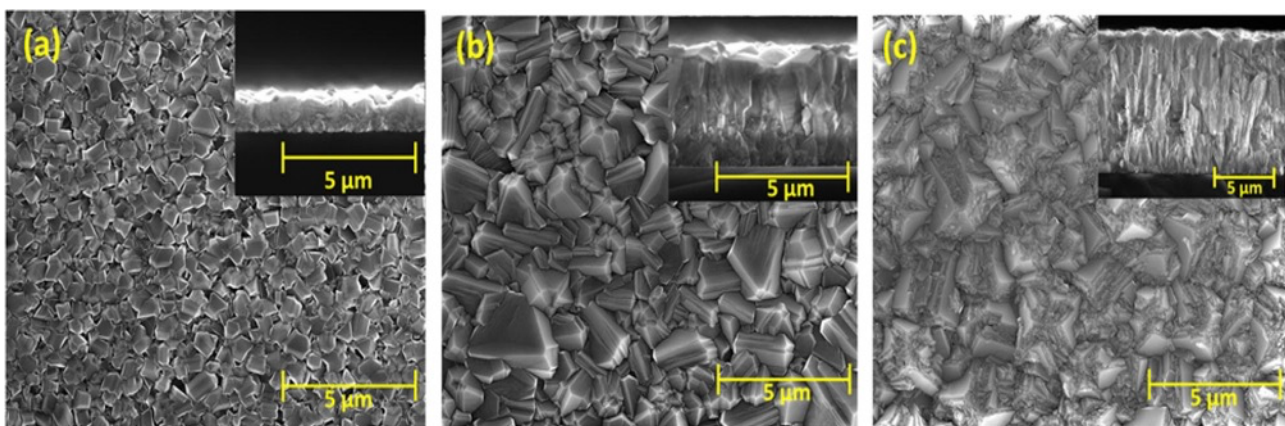


Figure 4. SEM micrographs of diamond films deposited on a silicon substrate for 8 hours using HFCVD with (a) 1.5%, (b) 3.0%, and (c) 4.5% methane in hydrogen. The insets are the cross-section SEM images.¹⁷

The substrate material must be able to withstand extreme temperatures however, most high melting point transition metals are not suitable due to their excessive reactivity with carbon-containing species. Molybdenum and especially silicon are popular choices due to their resistance to reactivity and their ability to form a thin carbide layer at the start of growth, which reduces stresses during growth. **Figure 4** shows examples of diamond films grown on a silicon substrate. Before growth, substrates generally require pre-treatment as diamond will not form spontaneously on foreign substrates. This is usually achieved *via* abrasion with fine diamond dust or coating the surface with nanosized diamond particles. This encourages

growth by increasing the density of suitable nucleation sites. Synthesis using pulse DC plasma does not require any nucleating aid, which is a key advantage for the production of devices on non-diamond surfaces^{1,10}

1.3.1 CVD Gas Phase Chemistry

A simplified growth scheme of CVD diamond is shown in **figure 5**, to begin the diamond surface is almost entirely saturated with hydrogen, limiting the number of suitable nucleation sites for hydrocarbon species (such as CH_3 radicals) to adsorb onto the substrate and blocking migration sites once adsorption occurs. Atomic hydrogen removes surface H giving rise to a suitable site, this will usually be filled by another H but occasionally gas phase carbon radicals will react, adding carbon, this process repeats until eventually a ring structure is formed. OH radicals are more effective at removing graphite than atomic H so if oxygen is present in the source gas mixture a higher quality diamond film is produced.^{1,11}

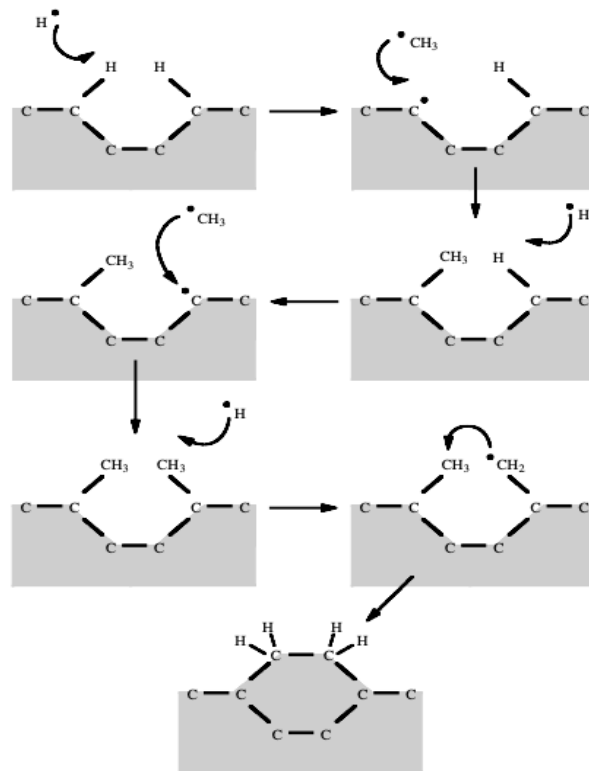


Figure 5. An example of one of the reaction processes occurring at substrate surface, in this case CH_3 is the radical species but other hydrocarbons can be used¹¹

The gas phase chemistry occurring during CVD growth has long been a focus of research, successful low-pressure growth has previously been carried out using a variety of precursor gas mixtures and compositions. Bachmann et al. found that the exact nature of the precursor gases was insignificant, however, the relative ratio of C/H/O in the precursor gas mixture

regulates deposition at standard operating temperatures and pressures. They condensed the findings of many CVD growth experiments to produce a C-H-O phase diagram (**Figure 6**).

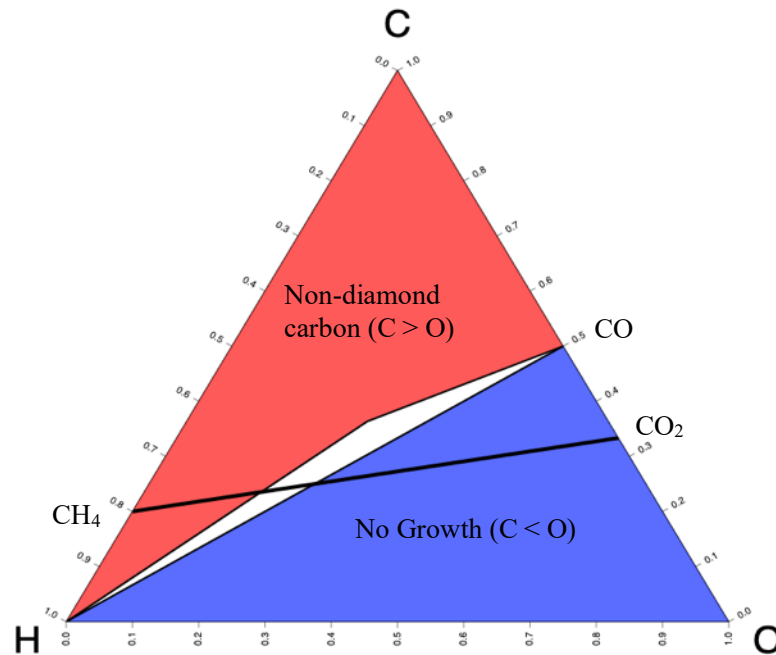


Figure 6. C-H-O phase diagram showing the relative ratios of the three elements where CVD diamond growth can be achieved. Adapted from Bachmann et al.¹⁸

Bristol University diamond group have conducted extensive simulations using a wide range of precursor gas combinations at a gas temperature of 2000K to investigate Bachmann's findings focusing on the regions within the phase diagram. The simulations revealed that for growth to occur, the CH₃ mole fraction must be high enough, approximately 10⁻⁶, and the H mole fraction must be sufficiently high to etch non-diamond carbon. These conditions are met in the white region centred around the C-O tie line, where the input mole fractions of carbon and oxygen are equal. Above this region, in the non-diamond growth region, the CH₃ mole fraction is high enough, but there is not enough atomic hydrogen present, leading to faster deposition than etching of non-diamond phases. Below the growth region, the CH₃ mole fraction is too low for growth to occur at around 10⁻¹⁰.¹⁸

1.3.2 Hot filament CVD (HFCVD)

HFCVD activation thermally activates the precursor gasses using a filament electrically heated to temperatures of around 2500 K, placed a few millimetres from the independently heated substrate (**Figure 7**). A sufficiently high melting point metal, which will not react significantly with the precursor gasses is required for the filament; tungsten and tantalum are examples of this.¹¹ The resistance of the filament is monitored, and supply voltage is adjusted accordingly to keep filament temperature steady.¹

The primary role of the filament is dissociating molecular hydrogen into atomic hydrogen, this occurs near the filament at higher pressures due to the high gas temperatures. The filament catalyses absorption of molecular hydrogen and desorption of atomic hydrogen at lower pressures, thermodynamics control the dissociation equilibrium.¹

Carbides will however eventually be formed through reaction with the precursor gas, resulting in the filament becoming brittle and limiting the maximum deposition time that can be done in one run. The flow rate of process gases is carefully monitored and controlled in the HFCVD process, using a vacuum chamber pumped continuously *via* a rotary pump, pressure is maintained at 20-30 Torr maintained by throttle valves.¹¹

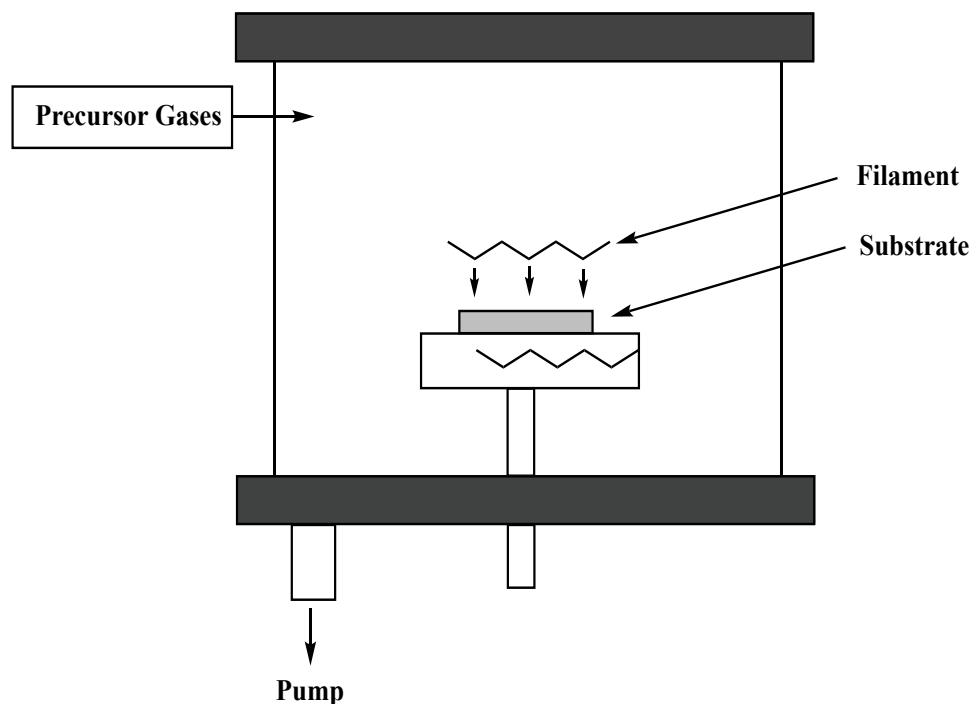


Figure 7. Simplified schematic of a CVD reactor using a hot filament to activate the precursor gases and deposit on the independently heated substrate, adapted from Gracio et al.¹

The HFCVD filament is sensitive to corrosive or oxidising gases, which therefore limits the precursor gas mixtures which can be used. It is also extremely difficult to avoid co-deposition of the filament material alongside diamond, this is not an issue for mechanical applications but causes issues with electrical applications. The operating temperature of HFCVD is

limited by the filament material so is carried out at lower temperature than plasma alternatives, this results in less atomic hydrogen production and therefore lower growth rates and reduces the effectiveness of biasing the substrate to induce orientated growth.^{1,11} Despite its shortcomings HFCVD growth is relatively straight forward, cheap to run, easily scalable and results in polycrystalline films of a reasonable quality so is a popular method of CVD synthesis.¹

1.3.3 Microwave Plasma Assisted CVD (MW PACVD)

MWCVD operates under similar growth conditions to HFCVD, in this system microwave power is coupled to the reaction chamber *via* a dielectric window to create a discharge as demonstrated in **figure 8**. Microwaves drive energy into gas phase electrons which subsequently transfer energy to the precursor gas through collisions. This process results in heating and hence fragmentation of the precursor gas into reactive H atoms and methane radicals, which in turn leads to deposition on the plasma immersed substrate.¹¹

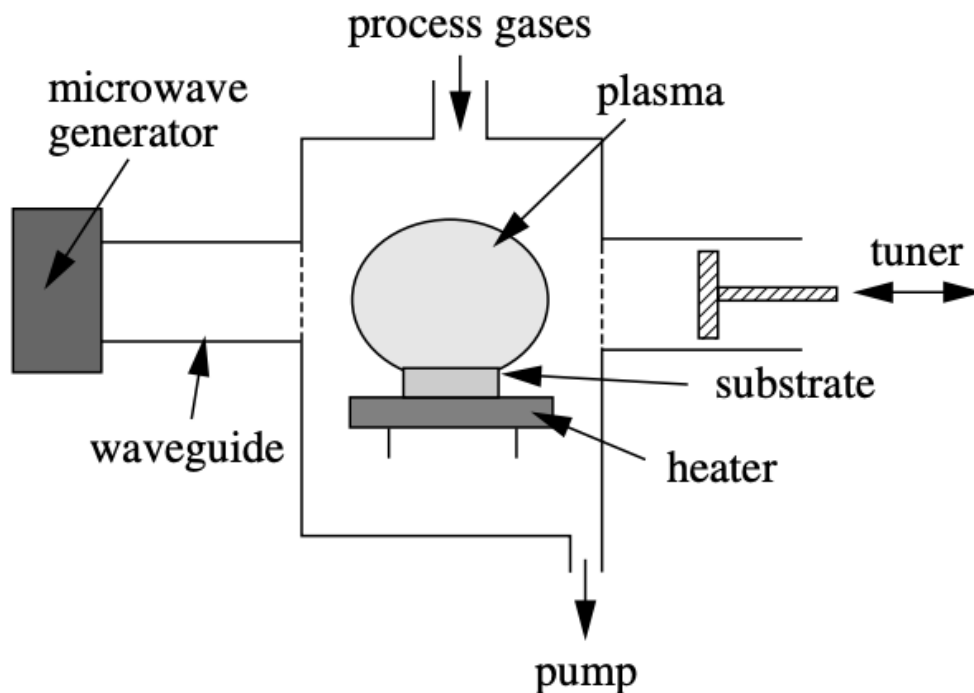


Figure 8. Schematic of the common 'NIRIM' type plasma MWCVD reactor, featuring the sliding tuner for adjusting the position of the plasma.¹¹

Although MWCVD is significantly more expensive than some of its counterparts, (such as HFCVD) it is widely used as there are a range of benefits to this synthesis method. MWCVD has less limitations as to the mixture of the precursor gas allowing gases with a high oxygen content or chlorinated gas to be used. It is an inherently cleaner system than HFCVD as having no electrode means there is no risk of contamination through filament erosion, MWCVD is therefore the preferred system for electronic applications. There is a substantial number of gas ions present in MWCVD which allows the possibility of biasing the substrate

to produce films with specific orientations. The plasma is restricted to the centre of the deposition chamber therefore preventing deposition of carbon on the walls of the chamber increasing efficiency, high power of MWCVD systems also means higher growth rates.^{1,11,15}

1.3.4 Pulse & DC Plasma Assisted CVD (DC PACVD)

First reported by Suzuki et al. in 1986, a DC plasma CVD system consists of a substrate located directly between an anode and cathode with a high potential difference.¹⁹ The substrate is immersed in a plasma created by electron bombardment which enables the activation of precursor gases. The electrical bias increases deposition speed by accelerating charged ions towards the substrate, and increasing the number of nucleation sites available on the substrate resulting in growth rates of up to 250 $\mu\text{m/h}$.²⁰

Much like MWCVD this method is cleaner than HFCVD due to eliminating metal impurities. The system is heated through a combination of electron bombardment and radiative heat from the plasma, external means of cooling the system are necessary because of this.¹ However, during DC PACVD growth the substrate sits on a powered electrode and is exposed to a plasma which has a higher electron temperature than during MWCVD growth. This leads to

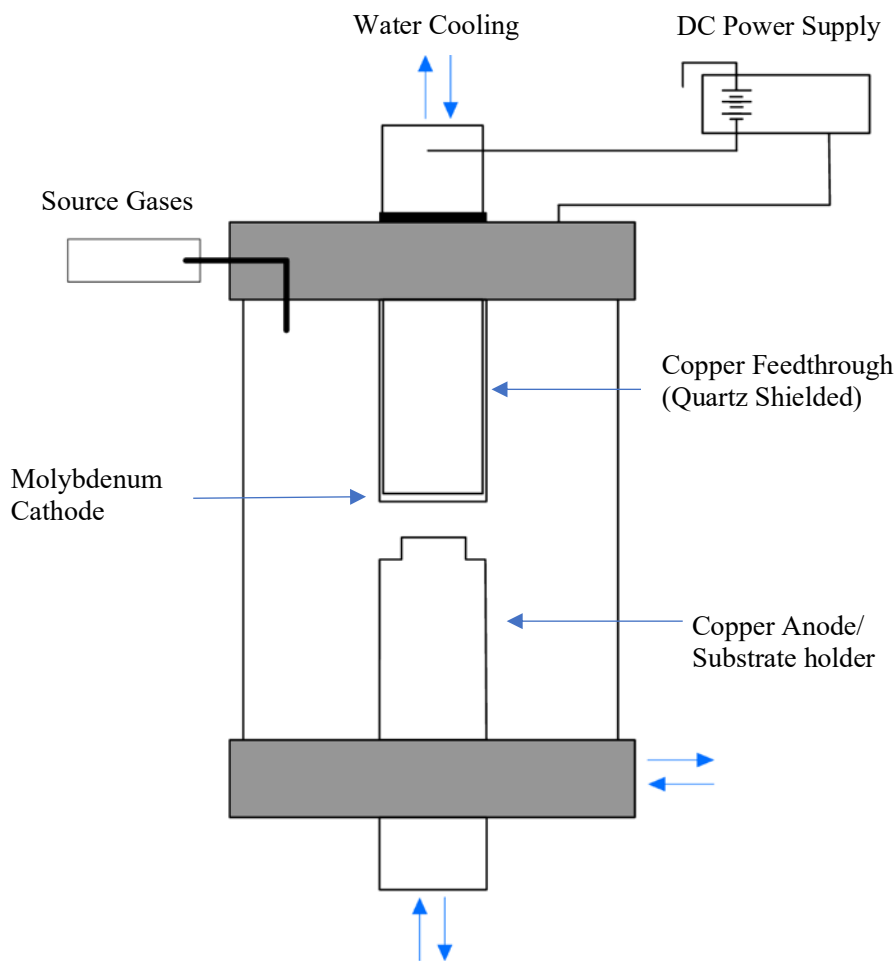


Figure 9. Simplified schematic of a pulsed DC CVD apparatus used by Hartmann et al.²⁰

increased production of atomic hydrogen from the same power input, resulting in faster growth rates and no requirement for pre-treatment of non-diamond substrates. Stability of the plasma across is a problem during DC-PACVD growth, this is caused by changes in the electrode material and uneven deposition during growth resulting in arcing of the plasma across the substrate. A pulsed power input was added by Hartmann et al. (**Figure 9**), pulsing power on for 72 μs then off for 50 μs . This pulsation increased the stability of the plasma, keeping the shape more uniform and limiting any potential arcing. This fast repetitive discharge produces different growth conditions from a constant power input and also opened the door for far larger substrates to be used.^{20,21}

Variation of the pulsed DC power supply parameters are key, they allow alteration of the gas phase chemistry occurring through changing the electron density or temperature, this therefore can be harnessed to offer a highly selective deposition process. If the pulsing frequency is incorrect the plasma can become unstable, leading to overheating and uneven distribution. A drawback of this method is that most commercially available power supply units are custom made, meaning they are expensive and the amount of control the operator has over the pulse conditions is limited.²²

1.4 Applications of Synthetic Diamond

The extreme control of CVD growth in terms of morphology and shape allows the remarkable properties of diamond to be harnessed through use in coatings and thin films. For this reason, CVD diamond is particularly useful for application in electrical devices such as high temperature diodes and solid-state detectors.¹

Physical systems that are suitable for use as qubits (units of quantum information) are crucial for the advancement of quantum computing. One such system that has been instrumental in the development of room temperature quantum computing is the synthetic diamond quantum

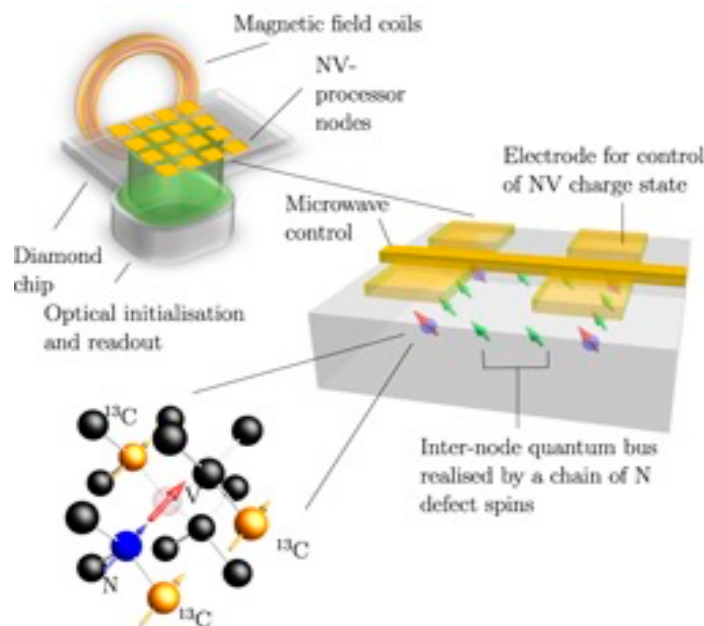


Figure 10. Schematic of a conceptual design of a diamond quantum computer. Each quantum processing node is formed by magnetically coupling an NV centre to an adjacent nuclear spin²⁴

processor, which comprises of a nitrogen valence centre and adjacent nuclear spins (**Figure 10**). These processors have shown excellent control, making them a promising candidate for large-scale quantum computing. However, continued optimisation of this technology is necessary to produce a scalable and reliable diamond quantum computer.^{23–25}

Synthetic diamond also offers solutions within modern electronics such as rapid electric vehicle chargers, which require exceptional thermal management due to their increasingly high-power density. Diamonds impressive thermal conductivity and high strength can be utilised in an interface with semiconductor materials such as GaN and Ga₂O₃ to enable high performance semiconductor solutions. The interface of heat spreading devices plays a crucial role in their performance. At the Centre for Device Thermography and Reliability (CDTR), led by Professor Martin Kuball, optical and Raman spectroscopy techniques are used to investigate the location and extent of heat loss. By optimising this interface, the production robust and lightweight heat spreaders can be achieved using CVD diamond wafers. This technology is being developed through integration with materials such as Gallium Oxide to produce more compact and efficient semiconductors.²⁶

1.4.1 Isotopically Pure Diamond

Natural diamond consists of 98.9 % ¹²C and 1.1 % ¹³C, it has been demonstrated that varying the isotopic composition of CVD diamond can alter its properties, which can be exploited for specific applications. Anthony and Banholzer found that thermal conductivity increases with increasing isotopic purity, to a maximum when the diamond structure is made up of pure ¹²C or ¹³C. Their findings concluded that the interatomic spacing decreased linearly as the ratio of ¹³C: ¹²C was increased. Infrared and Raman activity also varies between the isotopes, an increasing amount of carbon-13 in the diamond structure results in absorption bands with lower wavenumbers in the IR spectrum and a Raman peak at 1282 cm⁻¹ rather than the standard 1332 cm⁻¹ for natural diamond. This difference in Raman activity was harnessed by Qui et al to create pressure sensors using layers of isotopically pure ¹²C and ¹³C diamond films in an anvil cell.^{27,28}

A goal of CVD growth is using ¹⁴C methane stored in nuclear waste to produce isotopically pure diamond films, which can generate energy through beta decay and therefore be used in nuclear batteries. Although not a replacement for household batteries, beta voltaic batteries have a range of applications in long life devices that require a constant low power output and cannot easily be replaced such as in health monitoring of structures in the built environment for example smart concrete, space exploration and medical implants such as pacemakers.²⁹

Carbon-14 produces low energy beta emissions which are very weakly penetrating. The main concern for use of this isotope is the risk of internal exposure through production and inhalation of radioactive CO₂. Carbon-14 may also migrate through gloves and skin through the dead layer of the epidermis. Once in the body ¹⁴C is metabolised very quickly with highest exposure in body fat.³⁰ Using isotopically pure carbon is also expensive, carbon-13 methane is around 2.5 times more expensive than using regular methane as a precursor gas.³¹ In the synthesis of isotopically pure diamond films, it is essential to minimise both hazardous waste and costs. To achieve this, MW and DC-PACVD are more appropriate for producing ¹⁴C diamonds, as opposed to HFCVD, which requires disposal of the filament.

1.4.2 Boron Doped Diamond (BDD)

Doping semiconducting materials can increase their conductivity by several orders of magnitude, unlocking the vast potential for using CVD diamond films to produce electronic devices with exceptional properties. Unlike n-type doping with nitrogen, p-type doping of diamond can be readily accomplished due to the negative formation energy. This is achieved through the incorporation of boron containing gases such as B_2H_6 in the CVD plasma during growth. By adjusting the concentration of boron in the reaction chamber, the electrical conductivity of the resulting BDD film can be fine-tuned.

BDD is increasingly being used as electrodes in electrochemical redox cells. These electrodes are superior to their platinum counterparts due to their wide solvent window, low background current and ability to operate inertly without deterioration in harsh environments. It is key to maximise the surface area of these electrodes for optimal functioning, but this is difficult to achieve which therefore limits commercial availability of BDD electrodes. One potential solution to is growth of the BDD onto a porous material however, it is crucial to maintain both robustness and good conductivity in the resulting material.^{16,32,33}

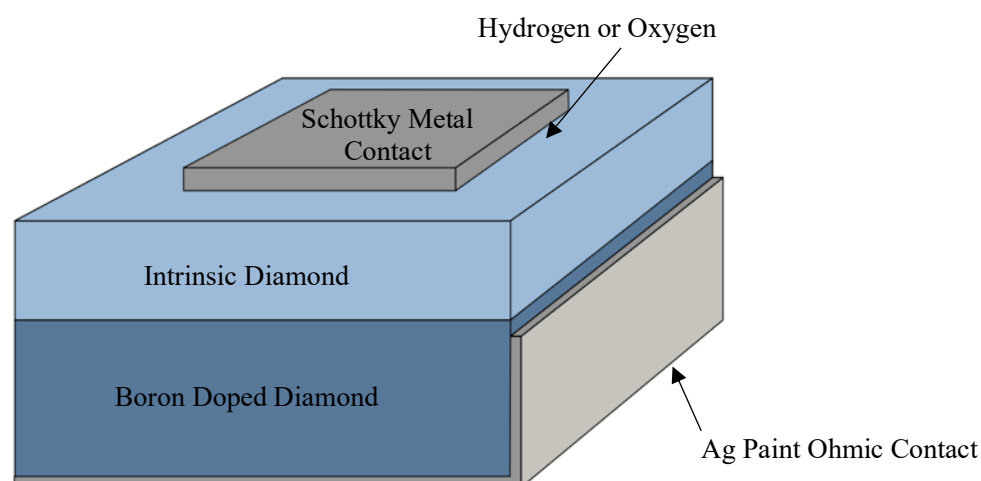


Figure 11. Schematic of a piM diamond diode construction, showing the intrinsic and boron doped layers of diamond which make up these devices, adapted from Liu et al.³⁴

The utilisation of semiconducting BDD to create piM diamond diodes (**Figure 11**), which incorporates both p-type and intrinsic layers in conjunction with a Schottky metal contact, has been demonstrated to exhibit exceptional diode performance. These diodes have the potential to revolutionise beta voltaic devices by integrating the radioisotope within the diamond structure, as opposed to an external configuration.³⁴

1.5 Static Flow

Ordinarily, CVD growth is carried out using continuous flow methods consisting of a premixed source gas with process pressure maintained by ensuring the gas input and exhaust flow rates are equal. The effect of gas flow rates on morphology and growth rates of CVD had previously been investigated, reaching inconsistent conclusions.³⁵ Celli et al. carried out growths with varying residence times (time taken to refill the chamber to the desired growth pressure) and found although gas flow rate had some effect on Raman spectroscopy and X ray diffraction of the films produced other properties such as the thickness of the diamond deposited, and electrical resistivity remained largely the same, there is a lack of certainty as to whether flow has any effect on the films produced.³⁶

Successful CVD growth using a closed system hot filament reactor was demonstrated out by Lai et al. in 1995.³⁷ The focus of this research was to reduce the consumption of hydrogen during the deposition process, reducing costs of the films and improving safety of the process by minimising the amount of explosive hydrogen released into the atmosphere. To achieve this, CVD growth runs were carried out with a fixed amount of hydrogen, the carbon source was a graphite rod, suspended above the tungsten filament and no flowing gases were used during deposition. Through use of a combination of Scanning Electron Microscopy (SEM), X-Ray Microscopy (XRM) and Raman spectroscopy it was established that growth of CVD diamond films was successful under these conditions on both diamond and silicon substrates. The quality of diamond grown was reduced with increasing proportion of methane compared to hydrogen in the chamber. This was consistent with findings from standard flow CVD growth.

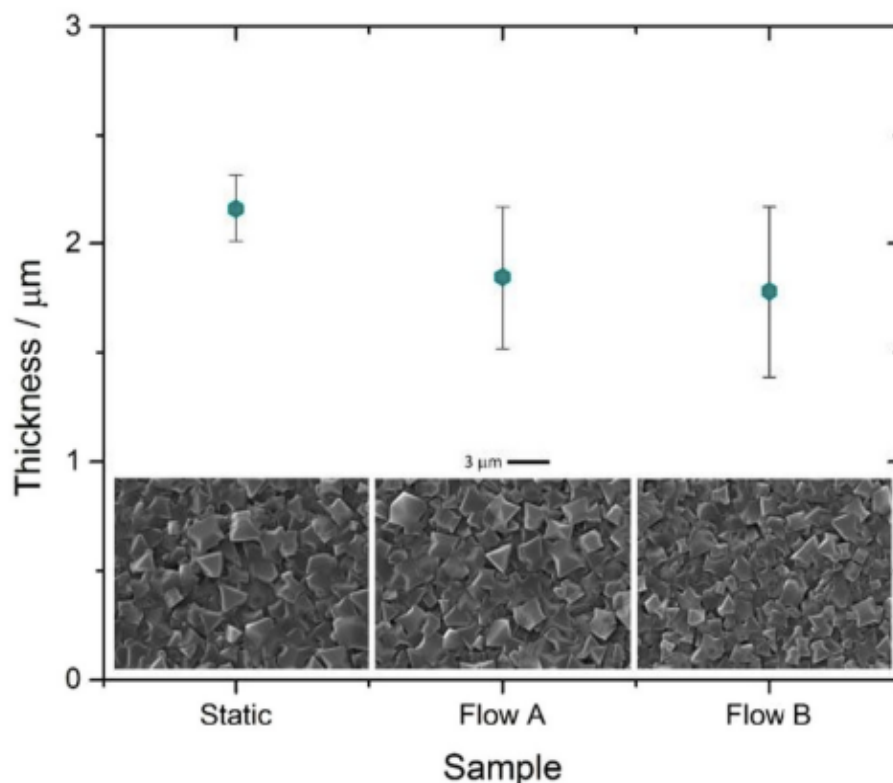


Figure 12. Thickness measurements of static and continuous flow growth runs alongside their corresponding SEM images.³⁵

Croot et al. sought to investigate using a sealed (static flow) precursor gas mixture for MW activated CVD growth.³⁵ Six growth runs were carried out, four of which sought to investigate the effect of substrate temperature on growth with a growth time of 90 minutes, the other two were shorter growth times. The diamond films produced were characterised using Raman spectroscopy and scanning electron microscopy.

It was found, as shown in **figure 12**, that the diamond films produced using this static flow precursor gas mixture were effectively identical to diamond films produced using traditional continuous flow CVD methods in terms of their sp^2/sp^3 ratio and crystalline morphology. The static flow growth runs yielded a 5.8 % conversion of carbon from the precursor gas into diamond, a near 30 times greater efficiency at $t = 90$ min. Croot et al. suggested that this could be further improved through the optimisation of the reactor and conditions used.

This distinctive method opens many doors for growth using expensive, hazardous or environmentally damaging precursor gases such $^{13}CH_4$ and $^{14}CH_4$ as exposure and waste is greatly limited compared to usual methods resulting in a lower risk, more cost-efficient synthesis process.³⁵ When carrying out static flow growth source methane is used as it is added, so concentration must be carefully maintained, if methane levels are too low the graphite etching rate will decrease resulting in an excess being deposited.³⁷

2. Experimental

2.1 Project Aims

The primary focus of this project was the commissioning of the mini pulsed DC PA-CVD reactor (mini-PDR) to synthesise diamond films under static flow conditions, first optimising conditions using ^{12}C then incorporating ^{13}C diamond. This reactor builds on from an existing PDR reactor in the school of Chemistry but, is designed for deployment by the UK Atomic Energy Authority (UKAEA) for growth using ^{14}C diamond within their active handling area.³⁸ The broader goal of this project is therefore to aid the development of beta-voltaic devices at this facility.

To achieve this, suitable operating conditions had to be established for the reactor. This included identifying power level conditions that ensure that the cathode remains within the desired temperature window for the mini-PDR. As well as assessing the stability and uniformity of the plasma whilst building up to these conditions. Once appropriate growth conditions are found a standard operating procedure (SOP) for the mini-PDR must be produced to ensure the users at UKAEA have a comprehensive guide for operating the reactor.

2.2 Mini-PDR

Several key factors had to be considered when designing the mini-PDR (**Figure 13**). It is essential to maintain temperatures of both the electrode and substrate within a range of 1050 - 1250 K so heat flow had to be carefully considered in the design. To achieve this, the aluminium chamber was water cooled using an ATC K3 chiller. The electrodes in the mini-

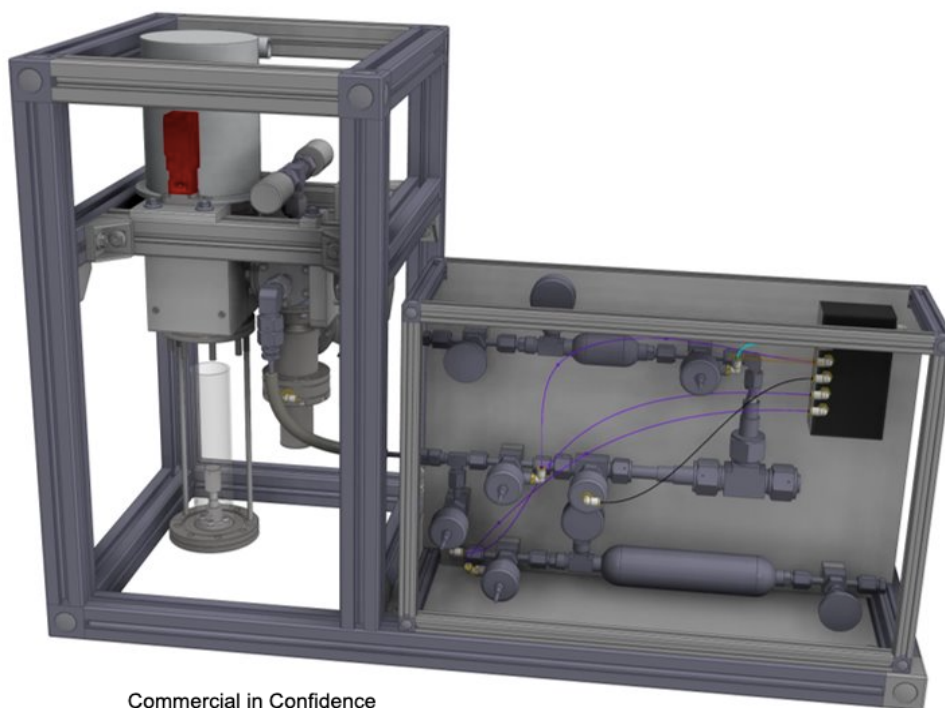


Figure 13. CAD drawing of mini-PDR reactor, designed for use by UKAEA to grow ^{14}C diamond from James Smith³⁸

PDR were made of replaceable molybdenum so they can withstand high temperatures, they are separated by a variable electrode gap of 18 ± 10 mm and feature a quartz tube to prevent the plasma arcing to the reactor walls. High voltage components in the reactor are shielded by a Teflon cover which also forms part of the safety interlock system. The mini-PDR also features sensors to detect the position of the pneumatically controlled valves and has an aluminium chassis to protect components from damage. The reactor was powered by an Advanced Energy Pinnacle Plus pulsed DC power supply unit (PSU). The mini-PDR was equipped with a burst disc to prevent overpressure in the chamber, a pressure measurement interlock and metal gaskets sealing all flanges to prevent any harmful gases from escaping. Chamber pressure can be monitored throughout the growth process on the mini-PDR using the Pfeifer ActiveLine Dual Gauge system, which was calibrated during manufacture.

The reactor typically operates using a 3-4% CH₄ / H₂ ratio, the source gases originate from the detachable board. This gas board was a requirement from UKAEA as it allows easy access to the *in situ* ¹⁴C vial breaking assembly. The hydrogen and methane accumulators were refilled as required to 1.5 Barr (gauge) using the existing lines from the Terminator reactor in the diamond lab.

Initially, the operating conditions used were based on the existing Balzer system in physics, a larger PDR reactor. The desired operating power was thought to be 800 W with the pulse frequency at 125 kHz. Plasmas were struck at a low pressure, then built up according to the script from the Balzer system to an operating pressure of 180 Torr (0.25 atm) alongside the power, a balance must be struck between low growth rates at low pressures, or increased power requirements and limited diffusion rates at high pressures.³⁹

2.3 Characterisation

The mini-PDR was equipped with various features to monitor reaction processes. These features include live camera imaging *via* the Basler Dart USB, a viewport that provides a direct view of the plasma, and the monitoring of spectral features throughout deposition. In addition, voltage and current inputs were also observed. Several test plasmas were struck assessing the plasma stability as the pressure and power inputs were increased, ensuring the plasma was evenly distributed and no arcing was occurring. Temperature readings were taken of the reactor externals using a thermocouple to ensure the reactor was not becoming dangerously hot.

As grown samples were characterised using a Renishaw 2000 laser Raman spectrometer. Raman spectrometry is extremely sensitive to surface morphology as each band directly corresponds to the vibrational frequency of a bond. This allows the characteristic diamond peak at 1332 cm⁻¹ to be clearly distinguished from the graphite G-band at 1582 cm⁻¹. Raman is therefore a valuable technique for determining both the nature and quality of material deposited.⁴⁰

2.3.1 Optical Emission Spectroscopy

Optical emission spectroscopy (OES) is an effective *in situ* technique for detecting and monitoring excited gas phase species such as atoms, ions, and molecules without affecting the plasma. The key species that were observed on the OES spectra during the test runs carried out are listed in **table 2**.^{41,42}

Table 2. The key species within the plasma observed by optical emission spectroscopy during the test runs, the wavelength at which they occur and the electronic transition responsible for each peak.^{41,42}

Emission Species	Wavelength / nm	Electronic transition
CN	388.3	$B^2\Sigma \rightarrow X^2\Sigma$
H γ	436.9	$5d^2D \rightarrow 2p^2P^0$
H β	486.3	$4d^2D \rightarrow 2p^2P^0$
C ₂	516.5	$d^3\Pi_g \rightarrow a^3\Pi_u$
H ₂	602.2	$3p^3\Pi_u \rightarrow 2s^3\Sigma_g$
H α	656.8	$3d^2D \rightarrow 2p^2P^0$

A Broadcom Qmini miniature spectrometer (**Figure 14**) was used for OES during this project. The spectrometer was set up with an exposure time of 1 s and to average across 5 exposures for each spectrum, this gave a reasonable balance between sensitivity whilst inhibiting excess noise. Spectra were continually observed during deposition using Waves spectroscopy software on a laptop connected *via* USB, these data were exported to Excel for the analysis included in this report.



Figure 14. The Broadcom Qmini spectrometer used to monitor how the optical emission spectrum varies during the deposition process.

3. Results & Discussion

3.1 Hydrogen only Tests

Before growth runs could begin on the mini-PDR several modifications were made to the reactor. The hydrogen chamber was removed and re-mounted using anti-seize compound to prevent cold welding of the bolts. The rubber gasket of the pressure gauge was replaced with an aluminium counterpart to satisfy the requirements of UKAEA. Prior to striking test plasmas, a leak in the hydrogen accumulator was identified and resolved by tightening the surrounding fittings.

Test I

The chamber was evacuated, refilled with 10.8 Torr of hydrogen and a plasma was struck at 150 W. Power and pressure were incrementally increased to 600 W and 61.5 Torr and the system was allowed to thermally equilibrate. The camera feed (**Figure 15**) showed the powered cathode glowing yellow/white, indicating a temperature in excess of 1000 °C.⁴³ If methane was introduced to the reaction chamber at this temperature a build-up of carbon on the cathode would occur. This is particularly detrimental in static flow mode of operation; it depletes the limited carbon supply thereby reducing deposition on the substrate. The stainless-steel electrode holders were replaced with more thermally conductive copper alternatives to improve heat flow and prevent overheating when operating at higher powers.

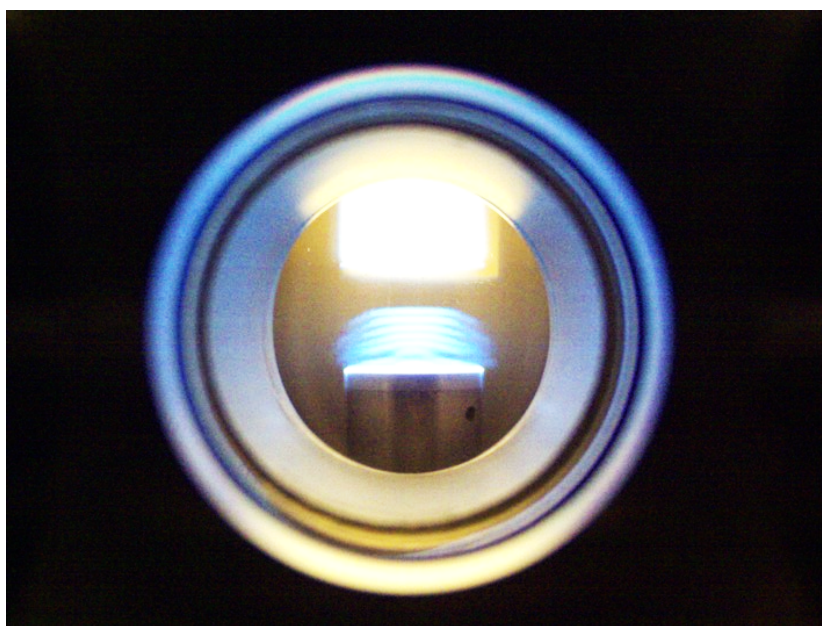


Figure 15. Image taken using the Basler Dart USB camera demonstrating the excessive temperature of the stainless-steel cathode holder. The cathode glowing white hot when the power was increased to 600 W, indicates a temperature above the desired operating window.

Test II

A plasma was struck at 200 W which was identified as a suitable power to strike at henceforth. Plasma stability remained consistent as the power and pressure were increased to 800 W and 170 Torr. Electrode temperatures were improved with the copper holders in place (**Figure 16**). The temperatures at the top of the heatsink and on the baseplate were 125 °C and 130 °C, respectively. This was not a concern as no-one will be in contact with the reactor whilst operating at UKAEA so burn risk is minimal. The striations observed in the plasma increased in density as power and pressure inputs increased, they are irregularities caused by fluctuation of the electric field during the pulsed-DC process. The shape of the plasma remained consistent throughout this experimentation. It was occasionally offset but centred between the electrodes as power and pressure were increased.²⁰

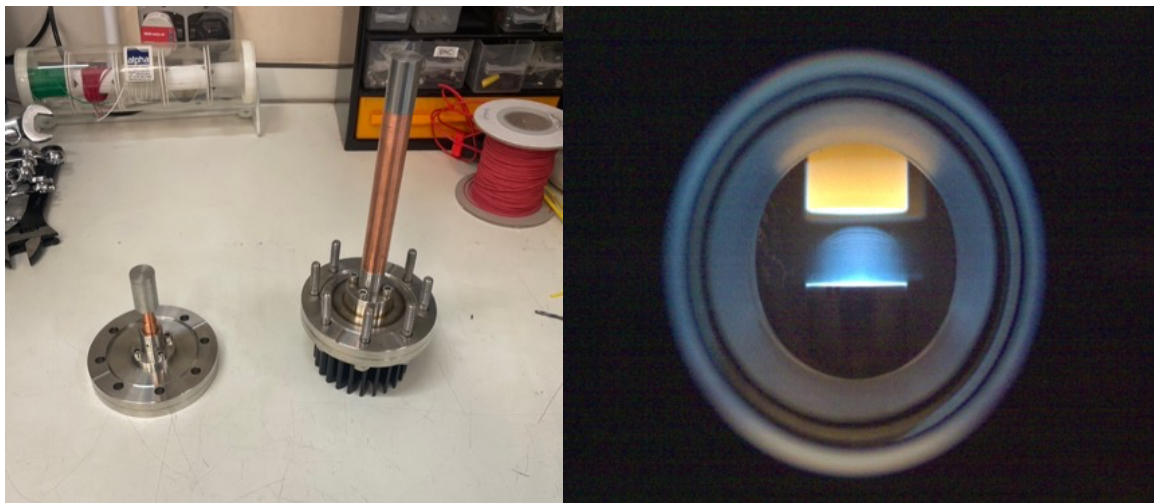


Figure 16. *Left: Image of the copper electrode holders which replaced the stainless steel. Right: Image of the pure hydrogen plasma test II with the copper holders in place, a more subtle red/yellow glow of the cathode indicates a more suitable temperature at a power of 800 W.*

Test III

Molybdenum discs, 5mm thick and 20 mm in diameter were used as substrates. Electrode separation had to be determined and adjusted accordingly to accommodate them. The electrode gap was measured at 17 mm which was insufficient with the substrate in place. This is because excess energy from the PSU would be directed towards heating the electrodes rather than maintaining plasma stability.

To avoid this, the copper anode was shortened by 5 mm. A plasma was struck with the substrate in place however, mounting the substrate on the anode proved challenging. A molybdenum bezel was incorporated to secure it (**Figure 17**) and all components were cleaned using propan-2-ol to remove contaminants before they were re-installed.



Figure 17. The molybdenum anode with the newly fitted bezel holding the substrate in place on top of the copper electrode mount.

3.2 Methane Containing Tests

Before methane could be introduced into the mini-PDR the gas board configuration was completed. The carbon-14 vial breaker was constructed by workshop staff, welding both end components to a length of $\frac{3}{4}$ " diameter stainless steel pipe. The methane chamber was assembled, mounted alongside the vial breaker (**Figure 18**), pneumatic tubing was connected to the control unit and the wiring was configured.



Figure 18. The fully assembled gas board configuration with the methane accumulator (Top), Vial breaking assembly (Middle) and hydrogen accumulator (Bottom) installed with pneumatics connected.

Test I

A vial containing 16 Torr of carbon-13 methane was inserted into the cracking assembly and fastened to ensure it was air-tight. The vial cracking assembly was backfilled with hydrogen to ensure no air was present in the system. Once operating power and pressure were reached the system was allowed to thermally stabilise and the vial breaker was operated successfully with OES verifying the presence of carbon in the growth chamber. After the reactor had cooled, the vial was carefully removed and was seen to have broken as desired (**Figure 19**).

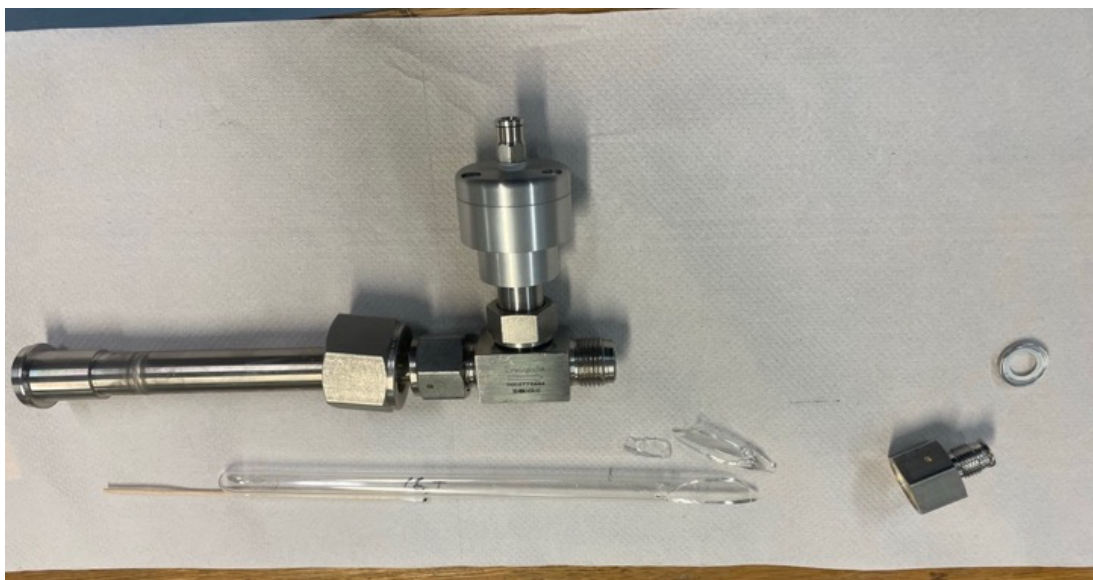


Figure 19. Vial breaker assembly after the successful breaking test alongside the broken ^{13}C methane vial.

Test II

A plasma was struck, power and pressure were incrementally increased to 800 W and 183.6 Torr, the function of the methane chamber was then successfully tested. However, this carbon appeared on the optical emission spectra in the form of a CN peak at 388 nm, overshadowing the hydrogen Balmer-alpha peak (**Figure 20**). This was a result of air contamination in the chamber, thought to be caused by expansion of components as power and therefore temperature increased.

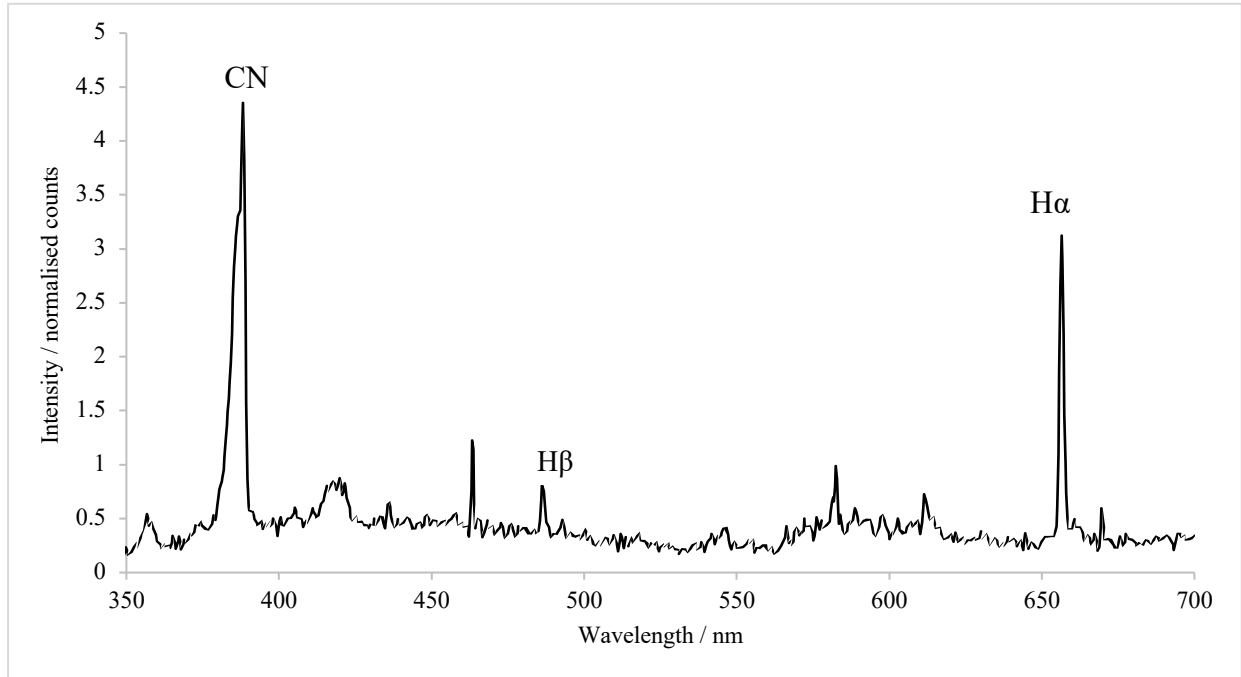


Figure 20. Optical emission spectra of the plasma once the methane was added to test II, the hydrogen Balmer series is clearly visible but overshadowed by the large CN peak at 388 nm.

Test III

The original quartz tube was replaced with one with a hole (**Figure 21**) to improve gas flow within the chamber. A plasma was struck, pressure was increased to 173.5 Torr at a lower power of 700 W to investigate if the chamber was still leaking at lower temperatures. 8 Torr of methane was then added to the chamber, CN was still present in the OES of this plasma.

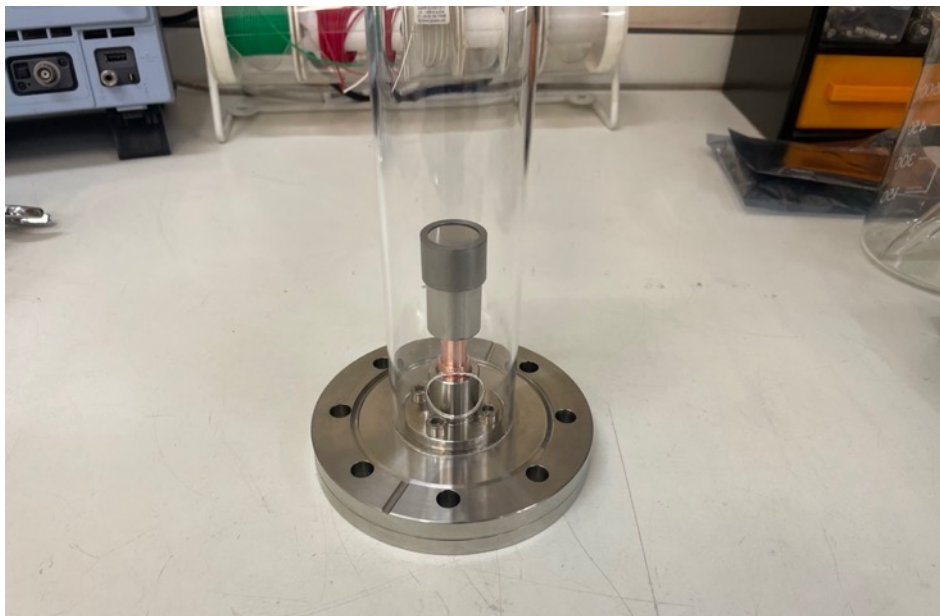


Figure 21. Anode fitted with the replacement quartz tube featuring the hole to improve air flow.

Another 6 Torr of CH₄ was then introduced to distinguish whether the first methane addition was quenched by a fixed volume of air in the chamber. The CN peak continued to grow indicating a leak causing the issue.

Test IV

The copper anode was then swapped back to stainless steel to achieve a higher substrate temperature at lower operating powers. This reduced heat flow to the baseplate therefore reducing the risk of leaks due to components overheating. A plasma was struck with this new electrode combination and a lower power of 600 W was used. Once the system had thermally equilibrated, 10.5 Torr of CH₄ was then added to 187.2 Torr of H₂ giving a concentration of 5.3%. CN was still observed on the OES, so power was reduced to 550 W in attempt to limit any potential leaks. Pulse frequency was reduced from 125 kHz to 100 kHz, observing the effect on plasma stability. The shape of the plasma remained consistent as methane was added. The striations faded slightly though variation was minimal, a pulse frequency of 125 kHz was deemed to provide a sufficiently stable plasma.

The reactor was left for 60 minutes to allow growth to occur (**Figure 22**). The chamber was evacuated, and the pump valve closed to investigate whether the vacuum was maintained at elevated temperatures. Pressure in the chamber increased, validating the presence of a leak to the vacuum chamber. The sample was removed with no deposition present.

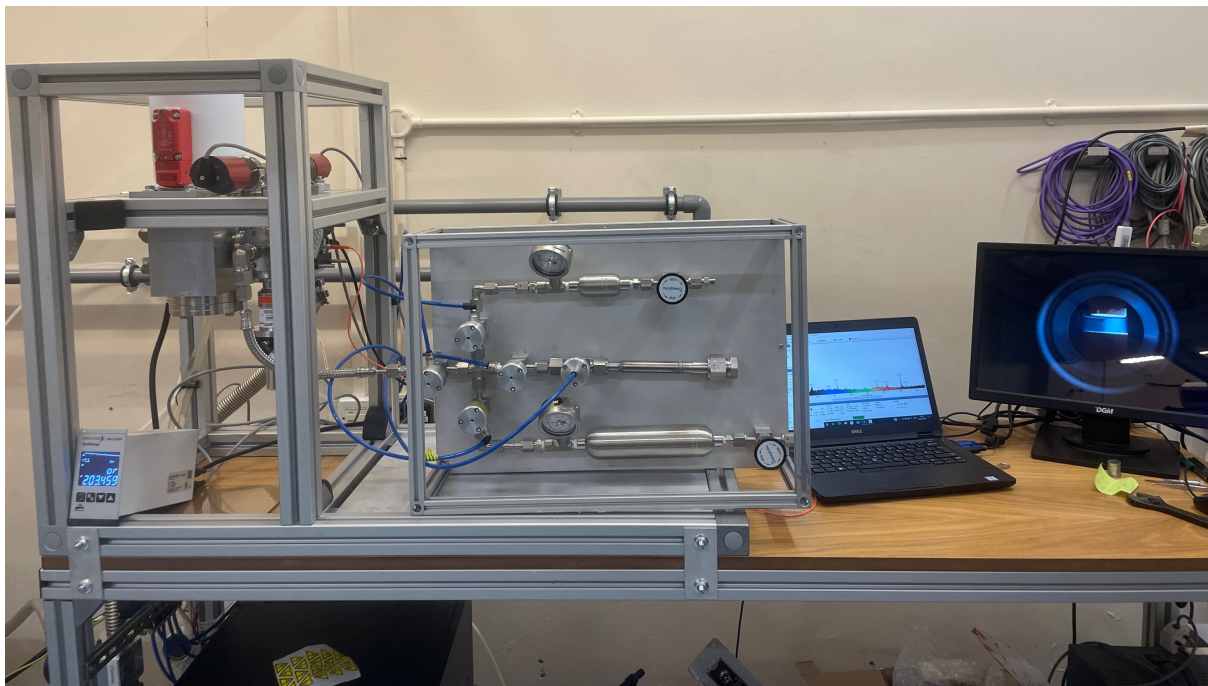


Figure 22. The mini-PDR reactor during test IV during the deposition period, the live camera feed can be seen on the monitor and the OES on the laptop screen.

Test V

Prior to this test metal gaskets between the chamber and heat sink were replaced and the bolts surrounding the chamber were tightened. The spectral sensitivity correction setting was also selected on the OES spectrometer. This accounts for the fact the spectrometer is more sensitive in the infra-red than visible region of the electromagnetic spectrum, resulting in more precise measurements. The spectrum was saturated, so exposure time was reduced to 0.1 s and averaging increased to 10 exposures, increasing sensitivity of the spectra by averaging across a greater number of exposures.

A plasma was struck, brought up to operating conditions and methane added. A small C_2 peak was present on the OES (**Figure 23**) though the CN peak remained. This was treated as a 'bake out' for the chamber, the temperature being sufficient to remove any air in the chamber and eliminate the possibility the CN peak was arising from a fixed volume of air in the chamber.

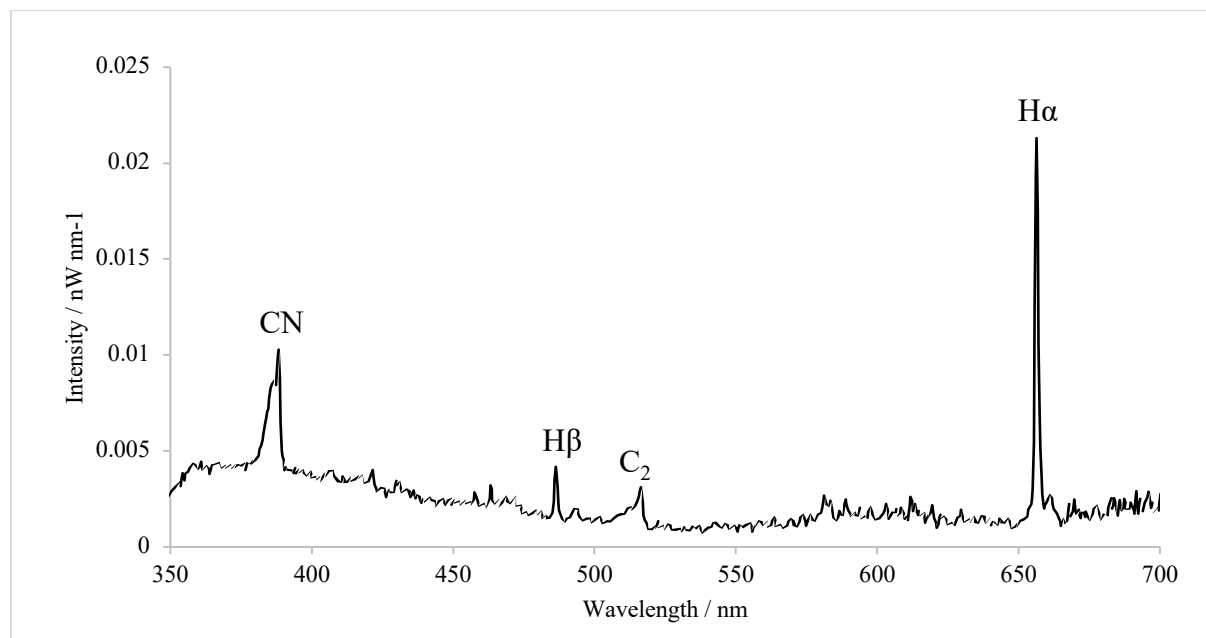


Figure 23. OES of test IV once methane was added, a peak was observed at 516 nm due to the presence of a C_2 dimer.

Test VI

After the 'bake out' a plasma was struck at 300 W and power/ pressure were increased to operating conditions of 182.8 Torr and 600 W. Methane was added, CN was still present on the OES but a small C_2 peak was also observed. The sample was left for 60 minutes to allow any potential deposition to occur.

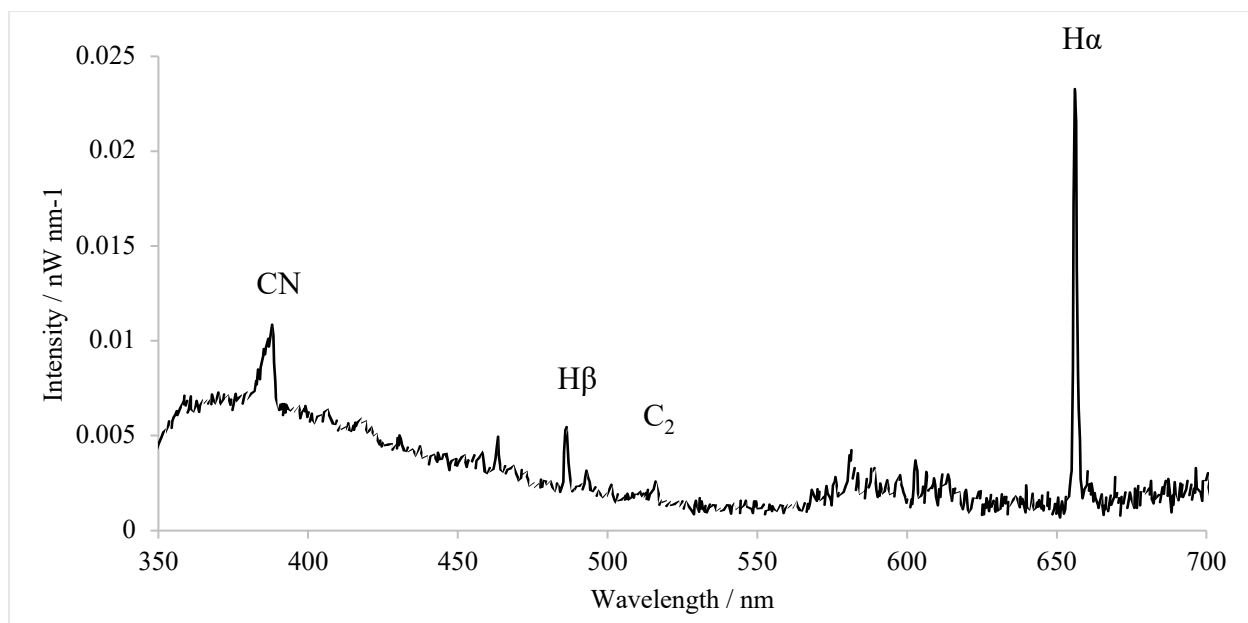


Figure 24. OES of test run V when methane was initially introduced into the reaction chamber.

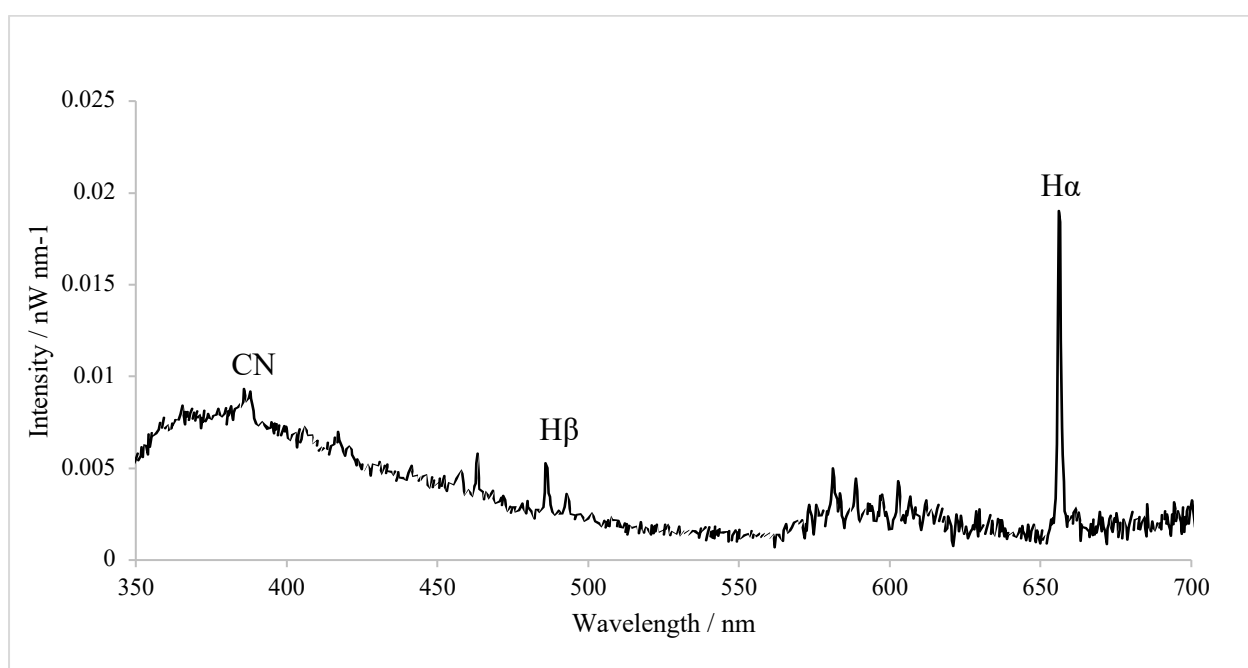


Figure 25. OES of test V after deposition was allowed to occur for 60 minutes, the CN peak has visibly depleted indicating the depositing of carbon in some form.

As can be seen from comparison of **figures 24 and 25** the CN peak depleted over the course of an hour indicating deposition occurred. The substrate was removed after allowing the reactor to cool. The sample was analysed using microscopy, small spherical graphite seeds were scattered across the substrate. A peak at 1582 cm^{-1} on the Raman spectra confirmed this deposited material was graphite rather than diamond.

This is because the excess nitrogen in the reaction chamber results in smaller facets with poor orientation or in this case graphitic deposits. It has been demonstrated that a N:C ratio of 0.4 is sufficient to deteriorate the surface morphology resulting in no crystal facets being deposited. This result suggested that the conditions used would be suitable for diamond growth once the chamber leak was resolved.^{10,44}

Test VII

The hydrogen and methane accumulators were filled using new tubing to eliminate the potential of contamination arising from the gas board. The fan shown in **figure 26** was positioned above the reaction chamber to reduce the external temperature of the reactor and thereby prevent the air leak occurring. A plasma was struck and built up to 600W and 182.8 Torr. 6.5 Torr of CH₄ was added giving a concentration of 3.43 % in H₂. The CN peak remained on the OES, so the fan had been unsuccessful in eliminating the leak.



Figure 26. The fan used in the unsuccessful attempt to cool the mini-PDR reaction chamber during test VII.

4. Conclusions

The primary focus of this project was the synthesis and characterisation of microcrystalline diamond diodes, formed on non-diamond substrates such as molybdenum under static flow conditions using the mini-PDR reactor. This would allow a method to be ascertained to produce high-quality diodes with reproducible electrical characteristics. To achieve this the mini-PDR firstly required conditions to be optimised using ^{12}C methane, followed by the incorporation of ^{13}C diamond capping layers onto the films with the aid of the vial cracking assembly. The successful production of such diodes would allow for the commissioning of this reactor at the UKAEA facility to produce beta-voltaic devices, utilising the procedures found.

Although no diamond films were successfully synthesised during this work, several key steps towards the deployment of the mini-PDR were undertaken. The carbon-14 vial cracking assembly was successfully constructed, mounted, and tested to function properly. This is a key element of the reactor which facilitates the safe addition of carbon-14 into the reaction chamber, this is essential to produce beta-voltaic devices at UKAEA.

Through observation of plasma stability during the test plasmas, both with pure hydrogen and introducing methane, appropriate growth conditions were established. An operating power of 600 W and pressure of 180 Torr were selected. These conditions were found to achieve adequate substrate temperature for deposition whilst avoiding the cathode overheating. This stopped unwanted carbon depositing on the cathode which would result in waste of the potentially limited feedstock gasses. Using these growth conditions deposition was successfully demonstrated onto a molybdenum substrate. The G-band at 1582 cm^{-1} on the Raman spectra identified this carbon as graphitic. This was due to the excess of unwanted nitrogen in the reaction chamber preventing the deposition of diamond.

The plasma tests enabled another project goal to be met, the production of a standard operating procedure for the mini-PDR to be used by UKAEA. Several crucial details were found to be included in the SOP such as the script for building up the plasma to growth conditions. This was based on the Balzer system in physics but adjusted to suit the mini-PDR, ensuring the plasma remained stable in terms of shape and uniformity throughout. An important consideration, letting the system thermally stabilise at 600 W and 160 Torr, until pressure plateaus before adding methane was also added to this document.

The main limiting factor in this experiment was a leak allowing air to enter the reaction chamber. After many failed attempts to eliminate the leak such as replacement of valves and use of a fan, it was not resolved. The nitrogen in the chamber quenched the methane added inhibiting successful deposition of sp^3 hybridised carbon and therefore diamond growth. This stopped comparison of characteristics of as grown samples based upon the growth conditions used, which was one of the stated goals for this project. The presence of air is particularly detrimental for the intended use of the mini-PDR as the feedstock gases are expensive or hazardous in the case of ^{14}C , therefore gas escaping must be prevented. Elimination of the chamber leak is therefore key for the progress of this project. This is being attempted through the fitting of an aluminium collar block extending the range of the water cooler, in theory preventing overheating and thereby the leak from occurring.

4.1. Future Work

Once the mini-PDR leak is eliminated, diamond growth will be carried out at the University of Bristol diamond lab before being deployed to its destination at UKAEA. Once successful synthesis is demonstrated integrating carbon-14 into the diamond films, the next stage of this work is the incorporation of tritium into the structure to further enhance the capabilities of these beta-voltaic devices. The UKAEA Hydrogen-3 Advanced Technology facility (H3AT), are looking to become world leaders in the production of these tritium based micro-power devices targeting the production of millions of devices annually. The production of these devices will play a role in the recycling of hazardous nuclear waste for a positive use, with estimates suggesting 50 kg of carbon-14 would produce of millions of devices. ⁴⁵

5. Appendices

5.1 Standard Operating Procedure

This document was produced in collaboration with James Smith as a comprehensive guide on use of the mini-PDR reactor. The tests carried out previously allowed the parameters used in this SOP to be reached. Some elements of this document still need to be updated with more information from UKAEA. The valve positions stated in this document are labelled in **figure 27**.

Cautions and warnings used throughout this document:



Hot Surfaces – Elements of the chamber (both internal and external) are subjected to temperatures exceeding 50°C. Caution should be taken to ensure all parts are at room temperature prior to handling.



High Voltages – During operation parts of the instrument are subject to high voltages. The PSU must be switched off, isolated and time allowed for internal parts to discharge prior to handling.



Compressed gases – Compressed air and other gases are used during operation. Ensure all sources are isolated and the system is depressurised prior to handling.



Flammable Gases – Flammable gases may be present within the chamber, exhaust and accumulators. Appropriate measures must be taken to prevent ignition.



Radioactive substance – Radioactive gases are used, and solids are produced during the use of this equipment. Appropriate precautions must be taken while handling the reactants and products.

System Checking Procedure

Prior to any use of the reactor the following checks must be made to the system.

- Ensure the Plasma PSU power connectors (feed and return) are both securely fastened. Check for any damage to the cable insulation.
- Ensure the chassis and chamber grounding cables are securely fastened.
- Ensure all interlocks are functioning.
- Ensure all thermocouples are in place and functioning.
- Ensure the pneumatic system is pressurised and operational.

- Make sure the vacuum system is operational and the base vacuum without gas load is within parameters.
- Ensure the extract system is functional and all interlocks are working.
- Ensure the closed-loop water cooling system is operational with flow interlocks functioning.

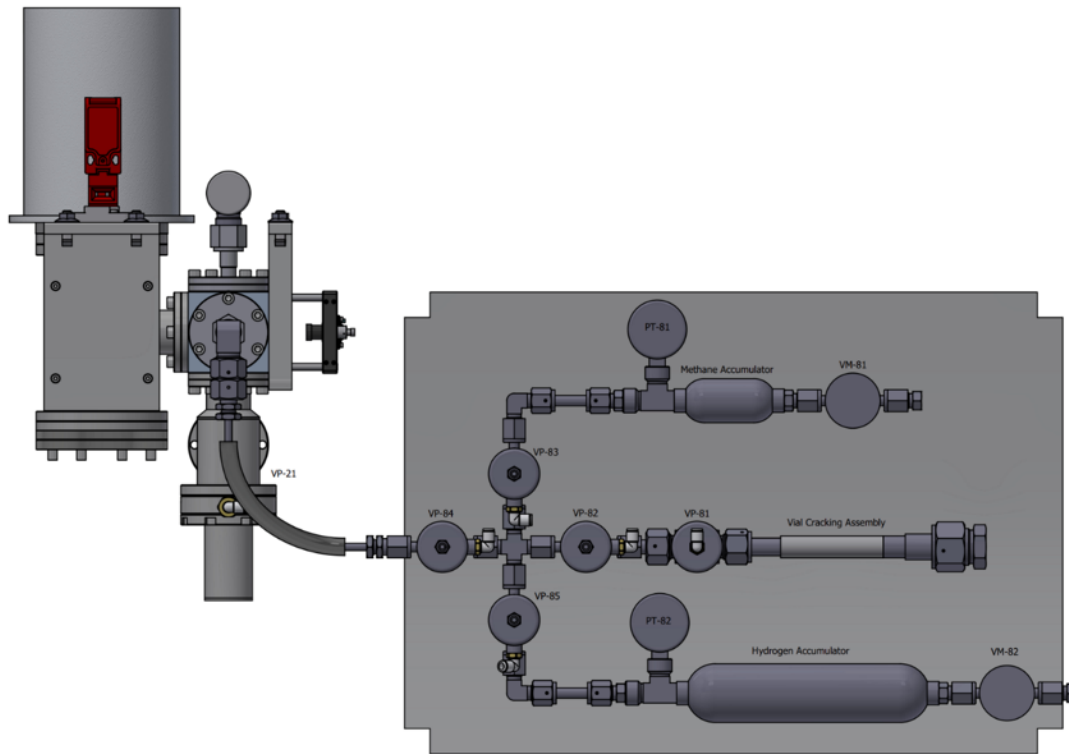


Figure 27. Schematic of the mini-PDR front chamber and gas board with pneumatic valves positions labelled.

Opening Chamber

This process is typically used to remove a grown sample after a growth run.

Prior to opening the chamber, the PSU must be switched off and isolated from the equipment. The chamber must also be at room temperature (measured on thermocouples Surface 1 and 2). The vacuum system must be operational, and a base vacuum registered on PT-21. All users must be wearing appropriate safety equipment prior to starting this procedure.

- Ensure pneumatic valves VP-82 to VP-85 are closed.
- Open VP-21 from the chamber to the vacuum pump system.

- Ensure PT-13 and PT-21 register a decrease in the chamber pressure, wait until a base vacuum pressure of $<2.0 \times 10^{-2}$ Torr is achieved.
- Close VP-21.
- Open air admit valves VP-12 and VM-12, the pressure in the chamber registering on PT-12 will rise to atmospheric pressure (approx. 760 Torr).
- Using a 13mm spanner loosen and remove the bolts holding the base of the chamber. Ensure the flange is supported during this process.
- Carefully remove the flange with the substrate assembly and quartz tube. Take care to lower the flange carefully to avoid damage to the quartz tube (**Figure 28**).
- Remove quartz tube from the substrate assembly flange.
- If removing the sample, ensure appropriate handling techniques are used.

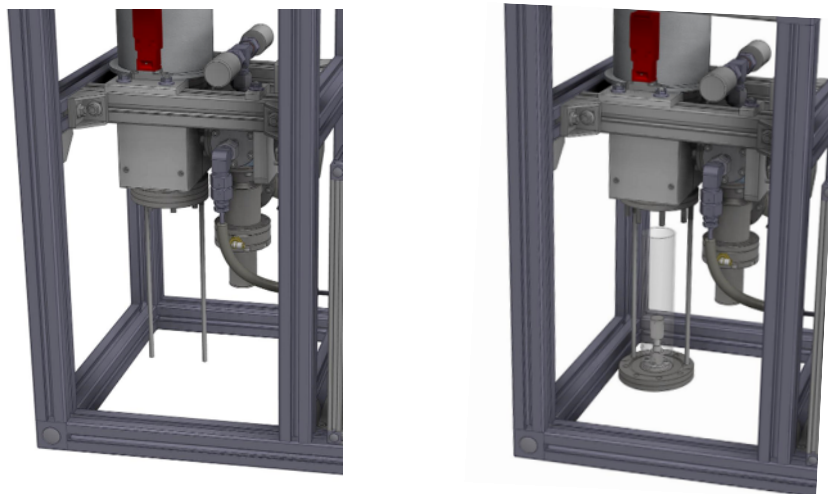


Figure 28. Schematics of the chamber base closed (left) and open with the substrate holder and quartz tube removed (right).

Chamber Loading

Prior to loading the chamber for a new growth run, ensure the system checking procedure has been carried out. Ensure the substrate, assembly and quartz tube are clean and dry prior to loading. The vacuum system must be operational, and a base vacuum registered on PT-21.

- Remove old CF gasket and replace with a new gasket (OFC CF 4.5"). Ensure gasket is centred and all knife-edges are clean and undamaged.

- Load new substrate onto the substrate assembly, ensuring good contact with the electrode. The substrate is retained and centred with a Molybdenum bezel that slides over the substrate and electrode.
- Carefully place quartz tube onto the substrate assembly.
- Raise the substrate assembly into position into the reaction chamber, carefully ensuring the quartz tube is not damaged.
- While holding the substrate assembly in position reinsert all the bolts into the base flange, firstly finger-tight, then tighten with a 13mm spanner in a star or opposite configuration. Ensure bolts are tight.
- Ensure air admit valves (VP-12 and VM-12) are closed.
- Open vacuum valve VP-21.
- After 5 minutes the pressure within the chamber, registered on PT-13 and PT-21, should reach base vacuum. If base vacuum is not reached during this time remove the flange, as per “Opening Chamber”, and then repeat this section.
- Reset all interlocks and ensure all interlocks are active.

Charging Gas Accumulators

This process must only take place after a “Chamber Loading” process has been completed as it requires a sealed chamber.

Warning - Care must be taken to ensure the chamber pressure never exceeds atmospheric pressure (760 Torr).

- Ensure the chamber is sealed, the vacuum system is operational.
- Ensure air admit valves (VP-12 and VM-12) are closed.
- Open VP-21.
- Wait until the pressure in the chamber has reached base vacuum (PT-21 and PT-13).

Evacuating the gas board accumulators

- Open VP-84. Wait until the pressure reaches base vacuum.
- Open VP-83. Any methane in the accumulator will be removed, wait until the chamber pressure reaches base vacuum.
- Close VP-83.
- Open VP-82. Any gas in the vial cracking assembly will be removed, wait until the chamber pressure reaches base vacuum.

- Close VP-82.
- Open VP-85. Any hydrogen in the accumulator will be removed, wait until the chamber pressure reaches base vacuum.
- Close VP-85.
- Close VP-84.

Growth Run

Prior to a growth run the substrate must be in place and the chamber sealed as per “Chamber Loading”. The system checking procedure must also be completed before starting this process. Checks should also be made on the pressures of gas in the hydrogen and methane accumulators prior to this process, if required carry out “Charging Gas Accumulators” before this process. Ensure the closed-loop water cooling is operational.

- Ensure the air admit valves VP-12 and VM-12 are closed.
- Open valve VP-21.
- Check vacuum on pressure gauges (PT-XX) ($<2.0 \times 10^{-2}$ Torr).

Hydrogen Flushing

- Open VP-84. Ensure pressure reaches base vacuum in cross section.
- Close VP-84.
- Open VP-85. Hold open for approximately a second, this allows hydrogen into the cross section.
- Close VP-85.
- Open VP-84. Wait until base vacuum is reached.
- Close VP-84.
- Repeat twice to ensure valves and lines are flushed.

Methane Flushing

- Open VP-84. Ensure pressure reaches base vacuum in cross section.
- Close VP-84.
- Open VP-83. Hold open for approximately a second, this allows methane into the cross section.
- Close VP-83.

- Open VP-84. Wait until base vacuum is reached.

- Close VP-84.

- Repeat twice to ensure valves and lines are flushed.

Vial Cracking Assembly hydrogen backfill

- Open VP-84. Ensure pressure reaches base vacuum in cross section.

- Open VP-82. Hold open, wait until base vacuum is reached.

- Close VP-84.

- Open VP-85. This backfills the vial cracking assembly with hydrogen. Hold VP-85 open for approximately a second.

- Close VP-85.

- Open VP-84. Ensure pressure reaches base vacuum.

- Close VP-84.

- Repeat to ensure valves and lines are flushed.

- With VP-84 closed, VP-82 open. Open VP-85 for approximately one second to allow hydrogen into vial cracking assembly.

- Close VP-82.

- Close VP-85.

- Open VP-84. Ensure pressure reaches base vacuum in cross section.

- Close VP-84.

The gas board is now ready to use for growth.

- Turn on Plasma PSU main power. Check PSU settings. Frequency = 125kHz, control = remote and regulation = power. Do not strike a plasma at this point.

- With VP-21 open check chamber is at base vacuum.

- Close VP-21. The chamber will now be sealed from the vacuum system for the duration of the growth process.

- Open VP-85. Introduces hydrogen into the cross section. Hold VP-85 open for one second.

- Close VP-85.

- Open VP-84. This will introduce a small volume of hydrogen into the sealed vacuum chamber, PT-13 should register approximately 10 Torr.
- On the Plasma PSU set the setpoint power to 200W. Strike a plasma by turning output ON. If plasma does not strike after 5 seconds, disable output to OFF. Wait until PSU output voltage has reached 0V then retry. In the event the plasma still does not strike, evacuate the chamber and restart this process. Check all connections and interlocks.
- On striking a plasma the PSU will display the output voltage and current and the camera will show a plasma between the two electrodes.

Building up plasma conditions

During the following process the chamber pressure is incrementally increased via operation of VP-84 and VP-85. To maintain a stable plasma the power is also increased when the pressure reaches setpoints (power follows the pressure).

From initial striking conditions, 200W at 10 Torr.

- Ensure VP-84 is closed.
- Open VP-85 for 1 second.
- Close VP-85.
- Open VP-84 for 1 second.
- Close VP84.
- Repeat this process until the chamber pressure reaches the setpoints outlined. On reaching the pressure setpoint the plasma PSU setpoint should be increased as per the following.

From 10 Torr, PSU setpoint = 200W

60 Torr reached, increase PSU Setpoint = 300W

100 Torr reached, increase PSU Setpoint = 400W

140 Torr reached, increase PSU Setpoint = 500W

160 Torr reached, increase PSU Setpoint = 600W

Once 160 Torr has been reached and plasma output power of 600W is achieved, the chamber must be allowed to thermally stabilise. During this time the chamber pressure will rise due to gas expansion. The pressure and surface temperature 1 and 2 should be monitored until each stabilise. Once thermal stability has been achieved a chamber pressure of approximately 180 Torr will be measured.

The spectrometer will detect the H-Balmer series emission from the pure hydrogen plasma.

Methane Addition

Methane is added into the chamber by operation of VP-83 and VP-84.

- Ensure VP-84 is closed.
- Open VP-83 for 1 second.
- Close VP-83.
- Open VP-84 for 1 second.
- Close VP-84.

During this process the chamber pressure will increase by approximately 4-10 Torr, depending on the methane accumulator pressure.

The spectrometer will detect a change in the plasma composition. The Balmer series will still be visible with the addition of emission from C₂ species.

Addition of gas from vial cracking assembly

The vial breaking assembly has been designed to add 14C methane into the chamber but can also be used to add 12C or 13C methane in prefilled vials. Addition of gas from the vial is via operation of valves VP-82 and VP-84, with the vial being broken via operation of an adapted normally open valve, VP-81.

Vial breaking and introducing gas to chamber

The vial cracking assembly must be flushed and filled prior to this process.

- Ensure VP-82 is closed.
- Open VP-84.
- Activate VP-81. This will activate the vial breaking valve.
- Open VP-82. The gas in the vial breaking assembly is introduced into the chamber.
- Hold VP-82 open for 1 second.
- Close VP-82.
- Close VP-84.

5.2 OES Data

The following optical emission spectra (**Figures 29 and 30**) highlight the presence of CN in the reaction chamber once methane was added. Further verifying the presence of a leak throughout this experiment.

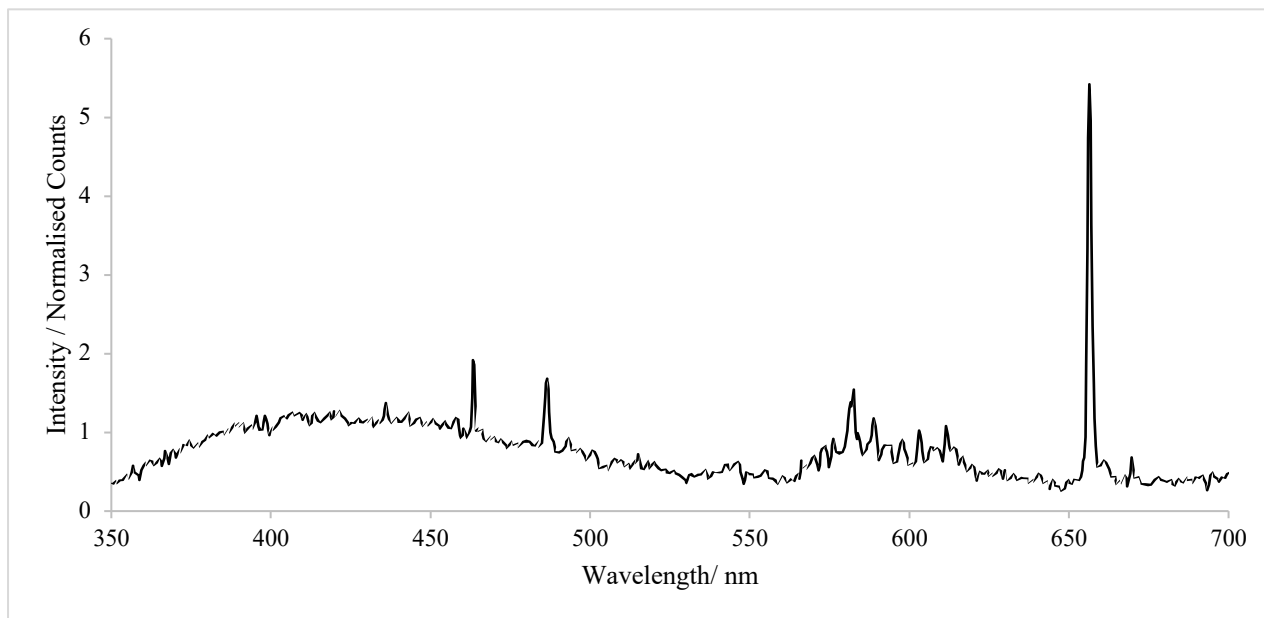


Figure 29. OES of test II before methane was added.

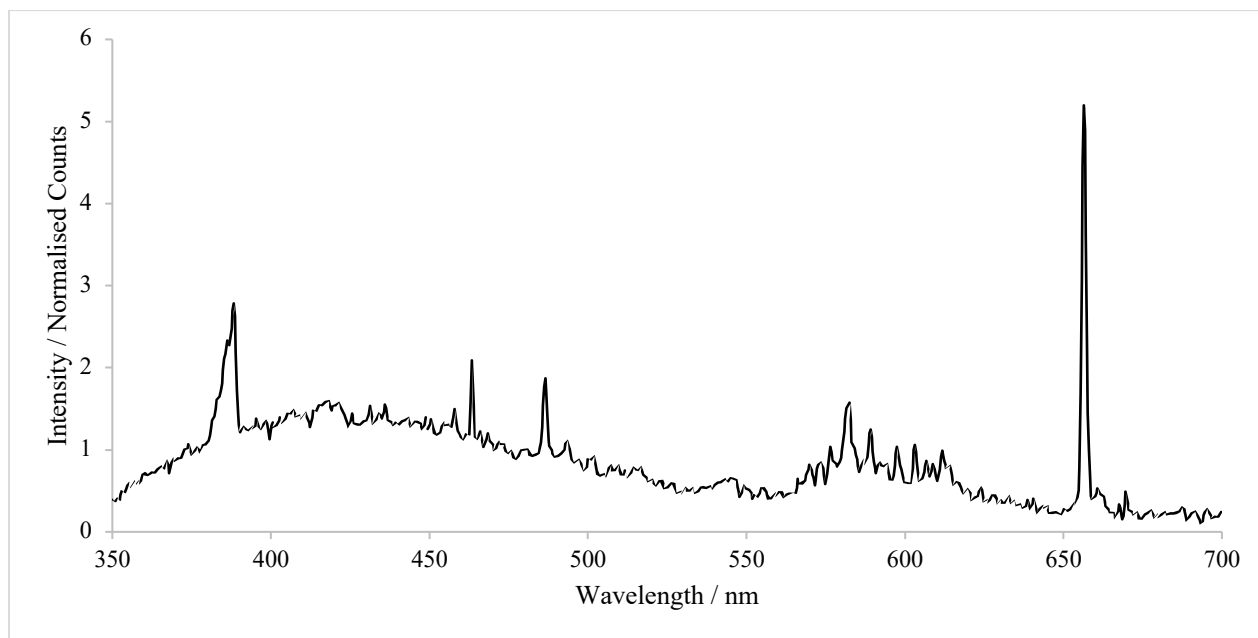


Figure 30. OES of test II after the addition of methane

6. Bibliography

- 1 J. J. Gracio, Q. H. Fan and J. C. Madaleno, Diamond growth by chemical vapour deposition, *J Phys D Appl Phys*, 2010, **43**, 374017.
- 2 J. Robertson, Properties of diamond-like carbon, *Surf Coat Technol*, 1992, **50**, 185–203.
- 3 J. A. Dean, Ed., *Lange's Handbook of Chemistry*, McGraw-Hill, New York, 14th edn., 1992.
- 4 S. Croft, Kaye and Laby – Tables of Physical and Chemical Constants (15th edn), *Physics Bulletin*, 1987, **38**, 149–149.
- 5 In *Group IV Elements, IV-IV and III-V Compounds. Part a - Lattice Properties*, Springer-Verlag, Berlin/Heidelberg, pp. 1–6.
- 6 Facts about diamond properties and applications, <https://www.additive.sandvik/en/diamond/facts-about-diamond-properties-and-applications/>, (accessed 23 November 2022).
- 7 J. E. Field, The mechanical and strength properties of diamond, *Reports on Progress in Physics*, 2012, **75**, 126505.
- 8 Y. A. Sorb, F. P. Bundy and R. C. DeVries, in *Reference Module in Materials Science and Materials Engineering*, Elsevier, 2016.
- 9 E. A. Ekimov and M. v. Kondrin, High-pressure, high-temperature synthesis and doping of nanodiamonds, *Semiconductors and Semimetals*, 2020, **103**, 161–199.
- 10 M. N. R. Ashfold, J. P. Goss, B. L. Green, P. W. May, M. E. Newton and C. V. Peaker, Nitrogen in Diamond, *Chem Rev*, 2020, **120**, 5745–5794.
- 11 P. W. May, Diamond thin films: a 21st-century material, *Philosophical Transactions of the Royal Society of London. Series A: Mathematical, Physical and Engineering Sciences*, 2000, **358**, 473–495.
- 12 J. Angus, in *Synthetic diamond : emerging CVD science and technology*, eds. K. Spear and J. Dismukes, Wiley, New York, 1994, pp. 23–24.
- 13 R. S. Balmer, J. R. Brandon, S. L. Clewes, H. K. Dhillon, J. M. Dodson, I. Friel, P. N. Inglis, T. D. Madgwick, M. L. Markham, T. P. Mollart, N. Perkins, G. A. Scarsbrook, D. J. Twitchen, A. J. Whitehead, J. J. Wilman and S. M. Woollard, Chemical vapour deposition synthetic diamond: materials, technology and applications, *Journal of Physics: Condensed Matter*, 2009, **21**, 364221.
- 14 M. N. R. Ashfold, P. W. May, C. A. Rego and N. M. Everitt, Thin film diamond by chemical vapour deposition methods, *Chem Soc Rev*, 1994, **23**, 21.
- 15 P. W. May, CVD diamond: a new technology for the future?, *Endeavour*, 1995, **19**, 101–106.
- 16 J. v. Macpherson, A practical guide to using boron doped diamond in electrochemical research, *Physical Chemistry Chemical Physics*, 2015, **17**, 2935–2949.
- 17 R. Ahmed, A. Siddique, R. Saha, J. Anderson, C. Engdahl, M. Holtz and E. Piner, Effect of precursor stoichiometry on morphology, phase purity, and texture formation of hot filament CVD diamond films grown on Si (100) substrate, *Journal of Materials Science: Materials in Electronics*, 2020, **31**, 8597–8606.
- 18 J. R. Petherbridge, P. W. May and M. N. R. Ashfold, Modeling of the gas-phase chemistry in C–H–O gas mixtures for diamond chemical vapor deposition, *J Appl Phys*, 2001, **89**, 5219–5223.
- 19 K. Suzuki, A. Sawabe, H. Yasuda and T. Inuzuka, Growth of diamond thin films by dc plasma chemical vapor deposition, *Appl Phys Lett*, 1987, **50**, 728–729.
- 20 P. Hartmann, R. Haubner and B. Lux, Deposition of thick diamond films by pulsed d.c. glow discharge CVD, *Diam Relat Mater*, 1996, **5**, 850–856.
- 21 Z. Wang and J. Zhang, Deposition of hard elastic hydrogenated fullerene-like carbon films, *J Appl Phys*, 2011, **109**, 103303.
- 22 M. A. al Mamun, H. Furuta and A. Hatta, Pulsed DC plasma CVD system for the deposition of DLC films, *Mater Today Commun*, 2018, **14**, 40–46.
- 23 S. Pezzagna and J. Meijer, Quantum computer based on color centers in diamond, *Appl Phys Rev*, 2021, **8**, 011308.

- 24 Y. Chen, S. Stearn, S. Vella, A. Horsley and M. W. Doherty, Optimisation of diamond quantum processors, *New J Phys*, 2020, **22**, 093068.
- 25 J. R. Weber, W. F. Koehl, J. B. Varley, A. Janotti, B. B. Buckley, C. G. van de Walle and D. Awschalom, Quantum computing with defects, *Proceedings of the National Academy of Sciences*, 2010, **107**, 8513–8518.
- 26 Diamond’s thermal management properties are enabling higher performance semiconductor solutions, https://e6-prd-cdn-01.azureedge.net/mediacontainer/medialibraries/element6/documents/bristol-case-study_18-11-21.pdf?ext=.pdf, (accessed 7 January 2023).
- 27 T. R. Anthony and W. F. Banholzer, Properties of diamond with varying isotopic composition, *Diam Relat Mater*, 1992, **1**, 717–726.
- 28 W. Qiu, N. Velisavljevic, P. A. Baker, Y. K. Vohra and S. T. Weir, Isotopically pure C13 layer as a stress sensor in a diamond anvil cell, *Appl Phys Lett*, 2004, **84**, 5308–5310.
- 29 ‘Diamond-age’ of power generation as nuclear batteries developed, <http://www.bristol.ac.uk/cabot/what-we-do/more-case-studies/2016/diamond-battery.html>, (accessed 18 December 2022).
- 30 Radioactive Materials Reference Sheet: Carbon-14, https://www.ehs.harvard.edu/sites/default/files/radioactive_materials_reference_sheet_c14.pdf, (accessed 11 December 2022).
- 31 Methane- 13C, Sigma Aldrich, (accessed 18 December 2022).
- 32 R. Kalish, Doping of diamond, *Carbon N Y*, 1999, **37**, 781–785.
- 33 H. Zanin, P. W. May, D. J. Fermin, D. Plana, S. M. C. Vieira, W. I. Milne and E. J. Corat, Porous Boron-Doped Diamond/Carbon Nanotube Electrodes, *ACS Appl Mater Interfaces*, 2014, **6**, 990–995.
- 34 B. Liu, B. Dai, K. Liu, L. Yang, J. Zhao, G. Shu, Z. Lv, G. Gao, K. Yao, M. Bi, J. Xue, W. Wang, V. Ralchenko, J. Han and J. Zhu, Alpha-voltaic battery on diamond Schottky barrier diode, *Diam Relat Mater*, 2018, **87**, 35–42.
- 35 A. Croot, E. J. D. Mahoney, H. Dominguez-Andrade, M. N. R. Ashfold and N. A. Fox, Diamond chemical vapor deposition using a zero-total gas flow environment, *Diam Relat Mater*, 2020, **109**, 108011.
- 36 F. G. Celi, D. White and A. J. Purdes, Effect of residence time on microwave plasma chemical vapor deposition of diamond, *J Appl Phys*, 1991, **70**, 5636–5646.
- 37 G. R. Lai, E. N. Farabaugh, A. Feldman and L. H. Robins, Deposition of Diamond Films in A Closed Hot Filament Cvd System, *J Res Natl Inst Stand Technol*, 1995, **100**, 43.
- 38 James Smith, *Mini PDR Preliminary Design Review*, 2021.
- 39 P. Hartmann, R. Haubner and B. Lux, Characteristics of a pulsed DC-glow discharge CVD reactor for deposition of thick diamond films, *Int J Refract Metals Hard Mater*, 1998, **16**, 207–216.
- 40 Joe Hodkiewicz, Characterizing carbon materials with Raman spectroscopy, *Thermo Fisher Scientific*.
- 41 K. J. Clay, S. P. Speakman, G. A. J. Amaratunga and S. R. P. Silva, Characterization of a-C:H:N deposition from CH4/N2 rf plasmas using optical emission spectroscopy, *J Appl Phys*, 1996, **79**, 7227–7233.
- 42 K. W. Hemawan and R. J. Hemley, Optical emission diagnostics of plasmas in chemical vapor deposition of single-crystal diamond, *Journal of Vacuum Science & Technology A: Vacuum, Surfaces, and Films*, 2015, **33**, 061302.
- 43 Steel Temper Colors: Temperatures & Explained, <https://www.servicesteel.org/resources/steel-tempering-colors>, (accessed 10 April 2023).
- 44 S. Jin and T. D. Moustakas, Effect of nitrogen on the growth of diamond films, *Appl Phys Lett*, 1994, **65**, 403–405.
- 45 Diamonds could be forever in nuclear-powered battery project, <https://ccfe.ukaea.uk/diamonds-could-be-forever-in-nuclear-powered-battery-project/>, (accessed 30 March 2023).

